Asynchronous Magnetic Bead Rotation (AMBR) for Biosensors

by
Paivo Kinnunen

A dissertation submitted in partial fulfillment
of the requirements for the degree of
Doctor of Philosophy
(Applied Physics)
in the University of Michigan
2011

Doctoral committee:

Professor Raoul Kopelman, Chair
Professor Roy Clarke
Professor Charles R. Doering
Professor Alan J. Hunt
Professor Bradford G. Orr

“Thou canst find of words a hundred,
Find a thousand wisdom-sayings,
In the mouth of wise Wipunen,
In the body of the hero;
To the spot I know the foot-path,
To his tomb the magic highway,
Trodden by a host of heroes;
Long the distance you must travel,
On the sharpened points of needles;
Then a long way thou must journey
On the edges of the hatchets.”
Wainamoinen old and trustful,
Well considered all these journeys

~

Sanoi vanha Väinämöinen: "Oi sie Antero Vipunen!
Ava suusi suuremmaksi, leukapielesi levitä,
pääsisin mahasta maalle, kotihini kulkemahan!"

Siinä virsikäs Vipunen itse tuon sanoiksi virkki:
"Mont' olen syönyt, monta juonut, tuhonnut tuhatlukuja;
moint' en vielä konsa syönyt, kuin söin vanhan Väinämöisen!
Hyvin laait tultuasi, teet paremmin, kun paloat."

Siitä Antero Vipunen irvisti ikeniänsä,
avoi suunsa suuremmaksi, leukapielensä levitti.
Itse vanha Väinämöinen läksi suusta suuritieon,
vatsasta varaväkevän, mahtipontisen povesta;
luiskahtavi poies suusta, kaapsahtavi kankahalle,
kuin on kultainen orava tahi näätä kultarinta.

An excerpt from the Kalevala,
the epic poem of Finland.
Translation by John Martin Crawford (1888).

For
my Mother Eeva Snellman and Father Ilkka Kinnunen
Sisters Tuuli and Veera
Brothers Kalle and Kuisma

ACKNOWLEDGEMENTS

I would like to thank everybody who has been part of the twenty odd years of my education and especially my advisor Professor Raoul Kopelman. First of all I like to thank my childhood education in Rovaniemi Rudolf Steiner School for nurturing my curiosity and my Mother who fought for the possibility of Steiner School elementary and middle school education in our city at that time - I was very fortunate to experience a long and careless childhood to which I credit many of my better traits.

Throughout my academic career I have received invaluable advice from my aunt and godmother Outi Snellman for which I am ever grateful, and without which this dissertation would most likely not have been written. One such advice resulted in me participating in an excellent exchange program in the University of Michigan during the senior year of my undergraduate program at the University of Turku. During the exchange I wrote my undergraduate thesis under Professor Bradford Orr, who saw potential in me that I didn't know existed. Thanks to him, I was able to join the Applied Physics program at the University of Michigan, which marks the start of the journey in which this document is a major milestone. I will remain grateful to him. I would also like to thank the excellent Applied Physics program, which I am very proud to be a part of.

Finding an inspiring project along with a good advisor and a mentor is a big part of completing ones doctoral degree. I have been most fortunate in choosing Professor

Kopelman as my advisor, who has unrivaled intuition and research philosophy. He let me do my own mistakes and learn from them, which I believe is a big part of academic education. A very important part in my academic career was also played by my lab mentor Dr. Brandon McNaughton who taught me the art of academic research. I joined the Kopelman research lab inspired by a seminar given by Dr. McNaughton, who had just recently graduated from the Kopelman laboratory (he was also in Applied Physics program). I am very grateful for all the advice and support he has given me over the years.

I would also like to thank all of my past teachers, friends and relatives and especially Irene Sinn for support. Kiitos!

TABLE OF CONTENTS

LIST OF FIGURES

LIST OF APPENDICES

CHAPTER I:

Introduction and overview

A high resolution, high throughput cell-growth/cell-stress biosensor that requires only small sample volumes could serve a wide area of biomedical research and applications. Such a biosensor would be invaluable for cell heterogeneity studies of clonal populations, antimicrobial susceptibility testing (AST), and drug screening. Certainly, new automated instruments for rapid and accurate recognition of bacterial resistance to antibiotics are needed, as noted in the review of contemporary AST practices [1]. While rapid molecular diagnostic methods exist, they have limited utility, and there is a need for rapid *phenotypic* measures of antimicrobial susceptibility [1,2]. On the other hand, while chemotherapy sensitivity and resistance assays (CSRAs) for cancer are not yet widely used in clinical decision making [3], they have a significant potential to be used for determining the correct therapy on an individual patient basis; as a result, novel rapid growth/stress sensors are needed.

Technologies with the resolution to observe single cell growth do exist, such as bright field microscopy, atomic force microscopy (AFM), scanning electron microscopy (SEM) and cantilevers; however, scalability and automation remain a major hurdle. Recently developed asynchronous magnetic bead rotation (AMBR) biosensors [4-9] possess

not only the high-resolution desired for the aforementioned biosensing applications, but also the high-throughput capability that the previously mentioned techniques lack. Furthermore, AMBR can be seamlessly combined with immunomagnetic separation, since the same magnetic particles can be used for both. In summary, AMBR biosensors show a great potential for various kinds of micro- and nano-growth studies, owing to their scalability, simplicity and nanometer scale resolution. The following sections discuss AMBR sensor applications from the Kopelman laboratory in more detail.

Historical context

Magnetic particles driven with rotating magnetic fields have interesting qualities that have found several applications in biomedical engineering (See Figure 1). Some of these applications are shown The applications include more traditional ones, such as magnetic microdrills [10,11], micromixing [12], and artificial bacterial flagella [13,14], as well as less straightforward applications, such as magnetic separation [15], background extraction [16], biomolecule detection [17,18], viscosity measurement [19], and AMBR biosensors [4-7,20].

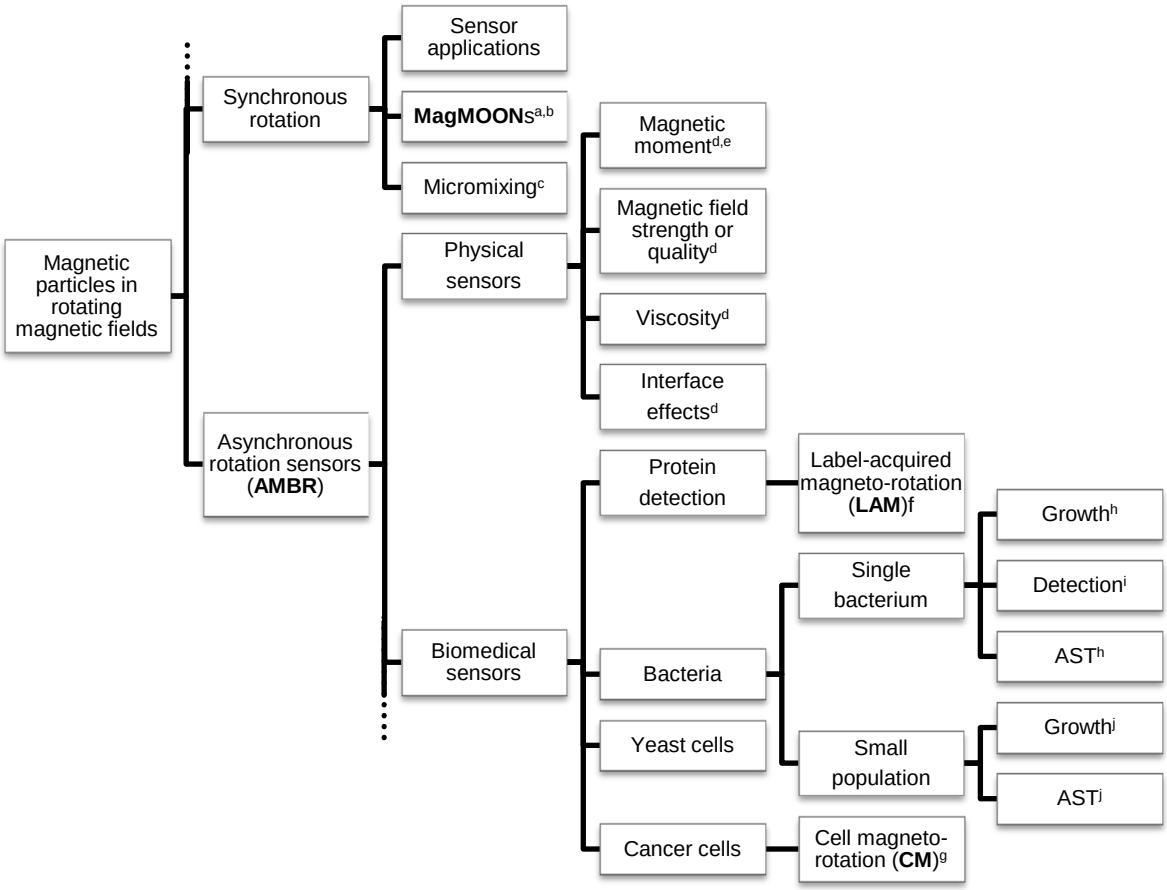

Figure 1: AMBR biosensor- and other applications of magnetic particles in rotating magnetic fields.

[a]Reference **[16]**	[f]Reference **[18]**
[b]Reference **[21]**	[g]Reference **[7]**
[c]Reference **[12]**	[h]Reference **[6]**
[d]Reference **[22]**	[i]Reference **[5]**
[e]Reference **[23]**	[j]Reference **[24]**

Another field worth mentioning in this context, and which precedes all the previously mentioned studies, is ferrohydrodynamics, where magnetic nanoparticle ensembles in rotating magnetic fields have been extensively studied. The first such study was conducted by Moskowitz and Rosensweig in 1967, where a ferrofluid was placed in a rotat-

ing magnetic field and its rotational rate was observed [25]. It was soon followed by a theoretical publication on single ferromagnetic (FM) and superparamagnetic (SPM) particles in rotating magnetic fields [26]. Caroli and Pincus theoretically predicted that there exists a critical frequency for FM particles, only below which the particles rotate synchronously with the rotating field, anticipating recent work, in 2006, conducted by McNaughton et al. Two decades after Caroli and Pincus's theoretical predictions, Popplewell et al., in 1990, using numerical integrations of the equations of motion, found that above the critical driving frequency the FM particle rotation rate is steady, but with a superimposed oscillatory component of relatively small magnitude; furthermore, the mean particle rotation rate decreases as the driving frequency increases [27]. This anomalous rotational phenomenon, where the magnetic particle rotates asynchronously with the driving field, is the basis of the AMBR biosensors; a full theoretical discussion can be found in the following sections.

AMBR biosensors

Ferromagnetic AMBR

A ferromagnetic particle has a tendency to align with an external magnetic field, and, therefore, at low driving frequencies, the magnetic particle rotates in synchrony with a rotating magnetic field. Above a threshold, known as the critical frequency, viscous forces of the surrounding fluid hinder the synchronous rotation, forcing the particle to rotate briefly backwards each time the driving field laps around the particle. In the case of two preferred orientations in the driving field (for example elongated superparamagnetic

particles [28] or optically driven nanorods [29]) the backward rotation occurs twice every time the particle is lapped by the field. An example of a ferromagnetic particle rotating synchronously (below the critical driving frequency) and asynchronously (above the critical driving frequency) with the external rotating magnetic field is illustrated in Figure 2 [4].

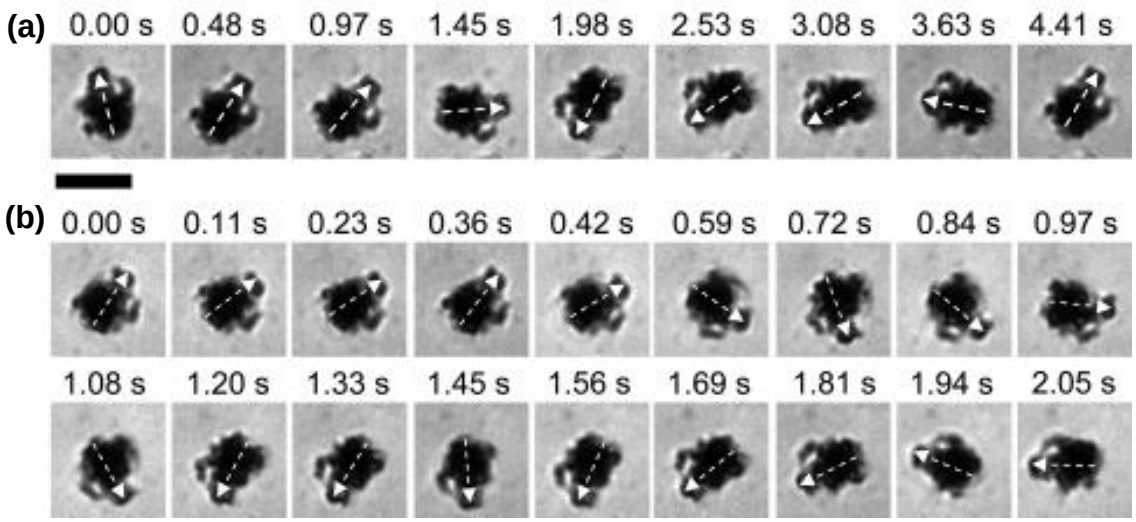

Figure 2: Sequence of bright-field microscopy images of a single magnetic particle, where the black scale bar is 7 um. (a) The particle is driven at below the critical driving frequency, progressing in the clockwise direction. (b) The particle is driven above the critical driving frequency. The particle begins in the clockwise direction, t = 0.00-0.23 s but then rotates in a direction that is opposite of the external driving field, the counter-clockwise direction, at t = 0.36, 0.84, 0.97, 1.45, and 2.05 s.

The critical frequency for an FM particle in a viscous solution, in an applied magnetic field, can be derived from the equation of motion, which is

$$I\frac{d^2\theta_{FM}}{dt^2}+\gamma\frac{d\theta_{FM}}{dt}=mB\sin(\phi) \tag{1}$$

where I is the moment of inertia, t is time, γ is the drag coefficient, m is the permanent magnetic moment of the particle, B is the magnetic field strength and ϕ is the phase lag, which is the angle between the external magnetic field (B) and the magnetic moment (θ_{FM}) [4,22,26,30,31].

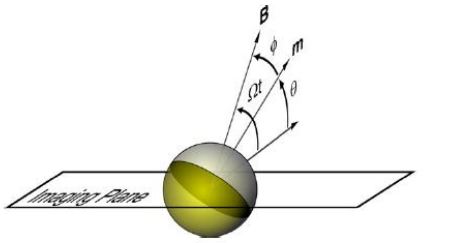

Figure 3: Schematic representation of a rotationally driven magnetic particle.

In a rotating magnetic field, the magnetic torque acting on the particle is $\Gamma_m = |\mathbf{m}\times\mathbf{B}| = mB\sin(\phi) = mB\sin(\Omega t - \theta_{FM})$, where Ω is the frequency of the rotating magnetic field. In low Reynolds number environments, the inertia term can be ignored and equation (1) can be written in a nondimensional form, which is the nonuniform oscillator equation:

$$\frac{d\phi}{d\tau} = \frac{\Omega}{\Omega_c} - \sin(\phi), \tag{2}$$

where $\Omega_c = mB/\gamma$, $\tau = \Omega_c t$, and $\phi = \Omega t - \theta_{FM}$. Below the critical driving frequency Ω_c, the particle rotates in synchrony with the driving field with a phase lag, defined by $\phi = \sin^{-1}(\gamma\Omega/mB)$. The maximum phase lag, $\pi/2$, occurs when $\Omega = \Omega_c$.

In the aforementioned systems, beyond the critical frequency there is a decline in the time-averaged particle frequency with increasing driving frequencies, with a well-characterized dependence of the average particle frequency on the driving frequency, namely:

$$\left\langle \dot{\theta}_{FM} \right\rangle = \Omega - \sqrt{\Omega^2 - \Omega_c^2}\,, \tag{3}$$

where $\left\langle \dot{\theta}_{FM} \right\rangle$ is the time average of the particle rotation rate. This relationship has been reported for magnetic particles in rotating magnetic fields, namely for magnetic hole systems [32], magnetorheological fluid droplets [33,34], magnetically loaded carbon nanotubes [35], ferromagnetic particles [4], and elongated paramagnetic particles [28]. Non-magnetic systems, such as optically driven nanorods, have also been reported to have similar frequency dependence [29].

While the dynamics of magnetic particles in rotating magnetic fields had been studied extensively, the first to recognize the potential of asynchronously rotating magnetic beads for biosensing applications were McNaughton et al. in 2006 [4]. The biosensing ability of the ferromagnetic AMBR biosensors stems from the fact that the critical frequency, Ω_c, is inversely proportional to the fluidic drag coefficient, γ, of the magnetic complex; namely,

$$\Omega_c = \frac{mB}{\gamma}\,, \tag{4}$$

where $\gamma = \kappa\eta V$, κ is the shape factor (6 for a sphere), η is the dynamic viscosity, and V is the total volume of the rotating body. Therefore a FM particle in a rotating magnetic field with a frequency above the critical driving frequency has a well-defined rotation rate, which depends on its effective volume ($V_{eff} = \kappa V$).

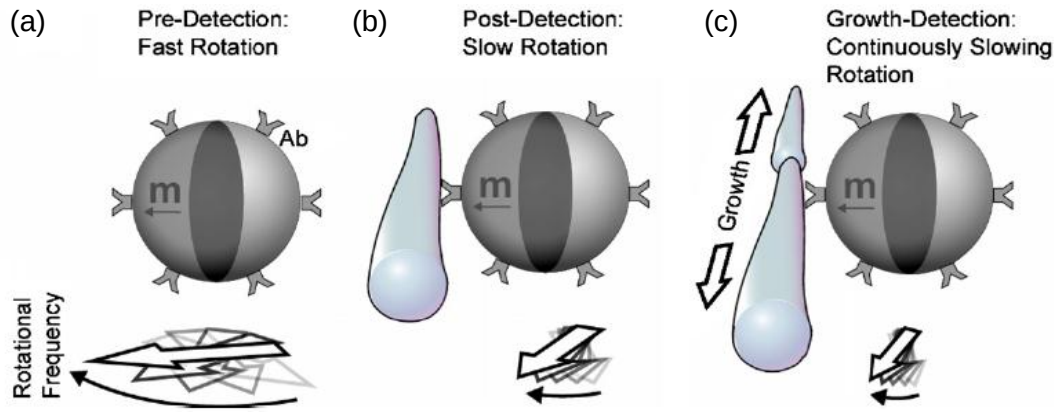

Figure 4: Schematic representation of a magnetic microsphere functionalized with an antibody with (a) no attached bacteria, (b) with one bacterium and (c) after bacterial growth. The rotation rate slows as more bacteria are attached or grow on the surface of the particle.

The effective volume can be solved using equations 3 and 4:

$$V_{eff} = \frac{mB}{\eta \left\langle \dot{\theta}_{FM} \right\rangle \sqrt{2\Omega / \left\langle \dot{\theta}_{FM} \right\rangle - 1}}. \tag{5}$$

In controlled environments, in which the temperature, magnetic field amplitude and frequency are constant, the effective volume can be calculated by measuring the rotation rate.

Similarly, the AMBR sensor may be used to measure other variables in equation 5, such as the viscosity, magnetic moment or magnetic field strength. It is also possible to use the phase lag of a synchronously rotating magnetic particle as a biosensor [36]. However, measuring the phase of a physical system is generally more difficult and less precise than measuring the rotational frequency.

Superparamagnetic AMBR

Magnetic particles that consist of a nonmagnetic particle matrix with embedded superparamagnetic (SPM) nanoparticles, possessing an induced rather than permanent magnetic moment, are preferentially used for immunomagnetic separation. A rotating magnetic field exerts a time invariant torque on a collection of SPM nanoparticles [37], and therefore these magnetic particles also lend themselves to AMBR biosensor applications. For instance, depending on the size distribution of its embedded magnetic nanoparticles, a given magnetic microparticle can exhibit ferromagnetic or SPM behavior in a rotating magnetic field. A ferromagnetic behavior will be apparent in the low amplitude and low frequency regime, while an SPM torque behavior will be dominant in a field with high amplitude or frequency. The total magnetic torque exerted on a particle in a rotating magnetic field can be written as:

$$\begin{aligned} \boldsymbol{\tau}_{mag} &= \mathbf{m}_{perm} \times \mathbf{B} + \left[\left(\chi' + i\chi'' \right) V_m \mathbf{B} \right] \times \mathbf{B} \\ &= m_{perm} B \sin\left(\Omega t - \theta_{FM} \right) \hat{\mathbf{e}} + \chi'' V_m \frac{B^2}{\mu_0} \hat{\mathbf{e}} \end{aligned} \tag{6}$$

where χ' and χ'' are the real and imaginary parts of the magnetic susceptibility, V_m is the magnetic content volume, μ_0 is the permeability of free space, and $\hat{\mathbf{e}}$ is a unit vector of the magnetic field. Variables in bold typeface are vector quantities. The real part of the susceptibility does not contribute to the torque because it is parallel to the applied magnetic field, and the cross product is zero at all times. The imaginary susceptibility, however, is perpendicular to the rotating magnetic field and the cross product is, therefore,

nonzero. The imaginary susceptibility is a property of the magnetic particle and has a frequency dependence that depends on the embedded nanoparticle size distribution. In the high frequency case, the contribution from the permanent magnetic moment can be negligible, and the first term on the right-hand-side of equation 6 is zero. Equating the SPM torque with the torque from the fluidic drag, the rotation rate of the particle can be solved:

$$\boldsymbol{\tau}_{drag} = -\kappa\eta V\dot{\theta}\hat{\mathbf{e}} \tag{7}$$

$$\boldsymbol{\tau}_{drag} = -\boldsymbol{\tau}_{mag} \tag{8}$$

$$\chi'' V_m \frac{B^2}{\mu_0} = \kappa\eta V\dot{\theta}_{SPM} \tag{9}$$

$$\dot{\theta}_{SPM} = \frac{\chi'' V_m B^2}{\kappa\eta V\mu_0}. \tag{10}$$

Note that the backward rotations that are present in the FM asynchronous rotation do not exist in the SPM case. Also, there is no explicit driving frequency dependence in the rotation rate of the particle; however, the imaginary susceptibility is a property of the magnetic material and usually is frequency dependent in nature. From equation (10) the effective volume can once again be solved for biosensing applications, yielding the effective volume of an SPM particle as a function of its rotation frequency:

$$V_{eff} = \frac{\chi'' V_m B^2}{\eta\mu_0\dot{\theta}_{SPM}}. \tag{11}$$

The general definition of superparamagnetism is that the magnetic moments average to zero over a finite time; usually a 100 second time scale is assumed (often implicitly) [38]. However, in a rotating magnetic field, the magnetic moments cannot relax and this definition does not apply; in this case, the natural distinction between permanent and induced magnetic moment is determined by which of the equations, (3) or (10), fit the frequency response of the rotating particle. Equation (3) describes the response of a ferromagnetic particle and equation (10) that of a superparamagnetic particle.

Biomedical applications of AMBR biosensors

Using the theory described in the above sections, the AMBR biosensors have been used to measure a variety of biological subjects and some of these experiments are discussed below.

Single bacterium detection

One of the first experiments revealing the high volume change resolution of the AMBR biosensor was on single cell detection. The binding events of an individual bacterium can be measured by observing the rotational rate changes of the AMBR biosensor [5], see Figure 5. The effective volume change of the rotating body, due to the attachment of a single bacterium, resulted in a 3.8 times slower rotational rate, on average.

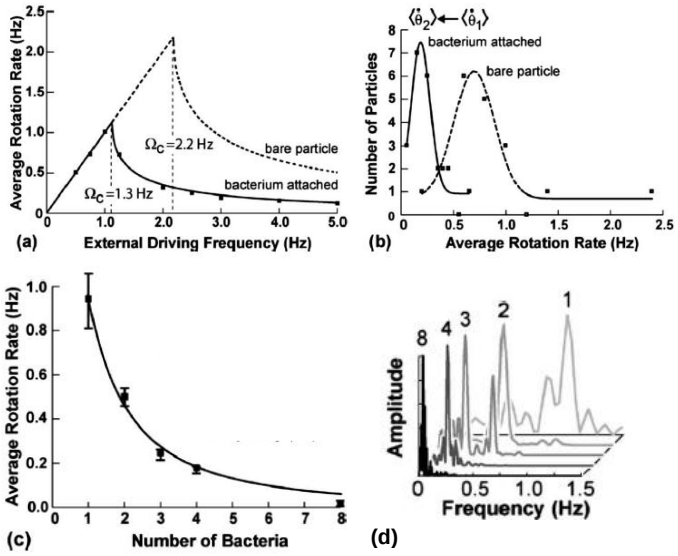

Figure 5: (a) The rotational response of a single magnetic microsphere with an attached bacterium at various external driving frequencies, where the squares are experimental data and the line is a theoretical fit to Equation (3), the dotted line is an approximated curve for a microsphere without a bacterium. (b) The average rotation frequency of 20 particles in a fluidic cell incubated with bacteria (solid curve) and a fluidic cell without bacteria (dashed curve). The magnetic microspheres with one bacterium attached rotated an average of 3.8 times slower than those without. (c) The average rotation rate of a magnetic microsphere dimer driven at 3.75 Hz, where 1, 2, 3, 4, and 8 bacterial cells were sequentially attached. The fit corresponds to the expected change in the nonlinear frequency, determined from Equation (3) for incremental additions of volume. (d) Normalized power spectral density of the intensity fluctuations of the dimer with 1, 2, 3, 4, and 8 cells attached sequentially corresponding to the data points in part c.

Single bacterium growth (nano-growth) and cell division

Optical microscopy offers the ability to measure the elongation of individual bacterium over multiple generations and it is currently the most widely used tool for studying single cell behavior [39-41]. However, the spatial resolution of far-field optical microscopy techniques is limited by the diffraction of light. Other high resolution tools that have proven useful for single cell analysis include scanning probe techniques [42] and cantilevers [43], but studies spanning multiple generations of individual cells have not yet been demonstrated with these techniques; furthermore, their optimal medium is air rather than water. As an alternative approach, we used superparamagnetic beads to monitor the

growth of individual bacterial cells, with 80 nm resolution for the cell length [6]. Due to the superparamagnetic nature of the particles, Equation (11) was used to measure how rotation-rate-changes translate into changes in effective volume of the sensor. The growth and division of individual *Escherichia coli* bacteria was observed, with 80-nm sensitivity to the cell length. Over the life cycle of a cell, up to a 300% increase was observed in the rotational period of the biosensor due to the increase in cell volume. In addition, we observed single bacterial cell growth response to antibiotics. Therefore this work demonstrates a non-microscopy based approach for monitoring individual cell growth dynamics, including cell elongation, generation time, lag time, and division, as well as their sensitivity to antibiotics.

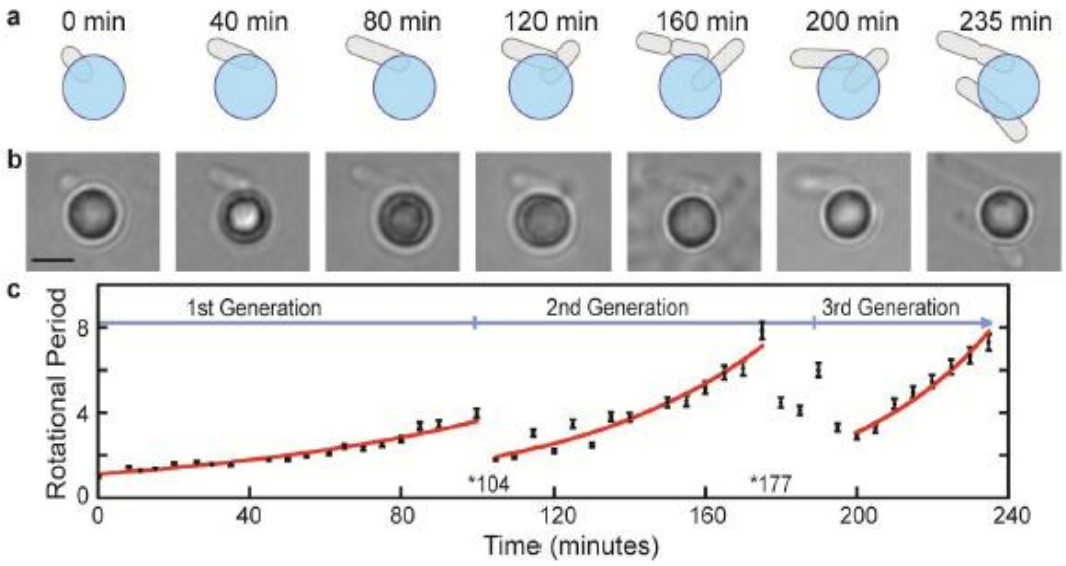

Figure 6: Growth and division of a single *E. coli* bacterium, measured with an AMBR sensor and observed with an optical microscope. (a) Schematic figures and (b) 100X oil immersion optical microscopy images of the magnetic particle sensor with initially a single bacterium attached and subsequent cell divisions. The scale bar is 2 μm. (c) Cell growth and division as observed with the AMBR sensor. After a period of growth, the first cell division is observed at 104 minutes and again at 177 and 199 minutes. The er-

ror bars correspond to the measurement error in the rotational period and the exponential fits are a guide to the eye. Data is normalized to 1 at time zero.

High frequency AMBR

Higher frequency asynchronous magnetic bead rotation allows better averaging, higher resolution and higher bandwidth studies, which will allow applications, such as real time single bacterium growth monitoring with sub-diffraction limited sensitivity and single virus detection, both in their given fluid environment. The relative uncertainty in bead radius of the ferromagnetic AMBR sensor is proportional to the relative measurement uncertainty and has no explicit frequency dependence. The sensitivity of the system is therefore:

$$S = \frac{r}{3} \times \frac{\Delta\langle\dot{\theta}\rangle}{\langle\dot{\theta}\rangle}, \tag{12}$$

where the sensitivity of the AMBR sensor, S, is defined as the smallest detectable change in the system's hydrodynamic radius r, and it is governed by the uncertainty in the bead frequency measurement, $\Delta\langle\dot{\theta}\rangle$. In order to measure the uncertainty of the bead rotation measurement, a 6.7 μm diameter magnetic bead AMBR sensor was driven with a 400 Hz, 1 mT, rotating magnetic field and was continuously measured over 37 seconds. The data is shown in Figure 7. The average rotation period was 25.4 Hz, with a 0.7 Hz standard deviation. Using these values and Equation (12) to calculate the sensitivity, the AMBR sensor was found to be sensitive to a 59 nm bead diameter change.

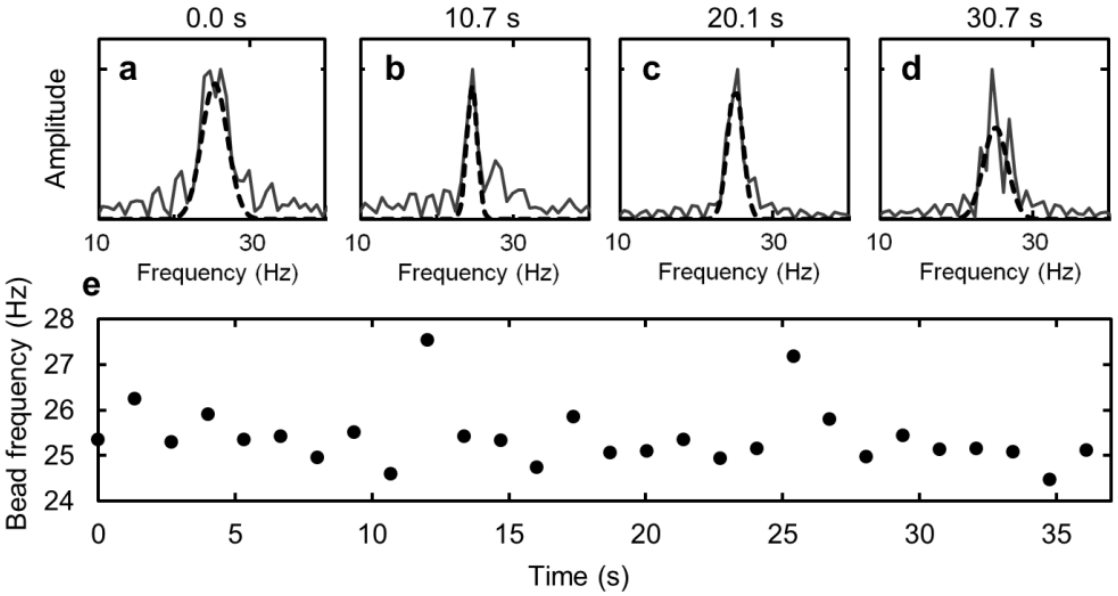

Figure 7: The AMBR sensor signal in time. (a-d) Fast Fourier Transform plots of rotation data, at time 0 s, 10.7 s, 20.1 s and 30.7 s. (e) The rotational period of the AMBR sensor in time, as measured with the Fourier analysis, examples of which are shown in parts a-d. The average of the bead frequency is 25.4 ± 0.7 Hz. The AMBR sensor is a 6.7 μm magnetic bead in 31 ^{o}C water.

Microfluidic integration of AMBR

Bead translation, magnetic interactions, surface adhesion and stiction are factors that may reduce the efficiency and accuracy of the AMBR biosensors under some experimental conditions [4]. By confining individual AMBR sensors within nanoliter-sized water-in-oil (w/o) droplets in a microfluidic channel, the magnetic beads are isolated within a defined space, separated from the neighboring beads, and separated from the channel walls by a thin oil layer. Microfluidic platforms also reduce reagent use and enable parallelization and high throughput due to their small dimensions. Therefore, integration of AMBR with microfluidics is advantageous in many respects. Sinn et al. microfabricated and characterized microfluidic channels to form droplets containing the maximum number of individual magnetic particles. The asynchronous rotation of the magnetic par-

ticles was characterized, concluding that water-in-oil droplets offer a good platform for AMBR studies with excellent stability and less stiction compared to glass surface, see Figure 8 (Sinn et al. to be published).

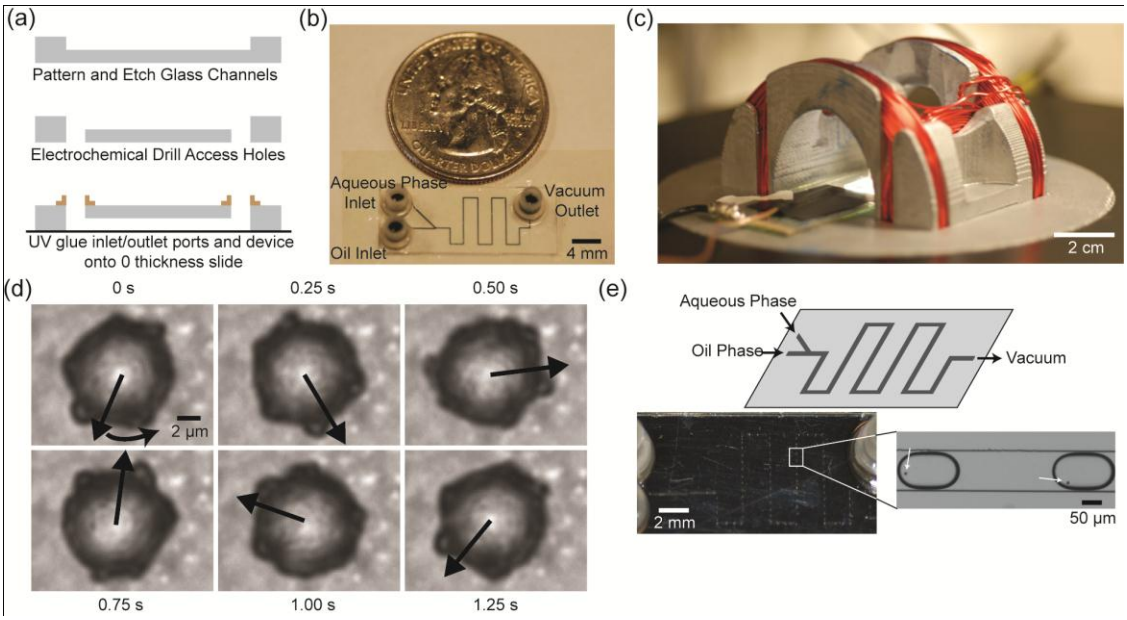

Figure 8: (a) Microfluidic glass channels are patterned and etched using standard glass lithography. Inlet and outlet holes are formed with electrochemical drilling. Device is UV-glued onto a 0-thickness cover slip and inlet and outlet ports are UV-glued to the access holes. (b) Image of the microfluidic droplet device. (c) A picture of the microfluidic device inside the electromagnet coils, which generate a rotating magnetic field of 0.9 mT amplitude at its core. (d) Optical microscopy image of an 8.8 µm magnetic bead rotating asynchronously with an external rotating magnetic field at a 50 Hz driving frequency, bead rotation rate being much lower (0.8 Hz). Visual aid is provided to observe the bead rotation. (e) Droplets of 0.5 nL to 1 nL in volume are formed by applying vacuum at the outlet and applying hydrostatic pressure at the oil inlet. A microfluidic device of this design holds between 50 and 75 droplets.

Small population growth and antibiotic susceptibility testing (AST)

Inappropriate antibiotic use is a major factor contributing to the emergence and spread of antimicrobial resistance. The long turnaround time (over 24 hours) required for clinical antimicrobial susceptibility tests (ASTs) often results in patients being prescribed

empiric therapies, which may be inadequate, inappropriate, or overly broad, prior to complete diagnosis. Reduction in the AST time would enable earlier and more appropriate therapies to be prescribed. A "Rapid AST" proof-of-principle study was done with AMBR biosensors in microfluidic water droplets, see Figure 9 (Sinn et al., to be published). AMBR biosensor droplet microfluidic platform was demonstrated, enabling single cell and small cell population growth studies for applications aimed towards rapid AST. A small cell population of uropathogenic *E. coli* was confined in microfluidic droplets and exposed to concentrations above and below the minimum inhibitory concentration (MIC) of gentamicin. Growth was observed for bacteria treated with gentamicin concentrations below the MIC; no growth was observed for bacteria treated with gentamicin concentrations above the MIC. A 100% difference in the sensor signal (ie. rotational period), was observed within 25 minutes between samples with and without antibiotics.

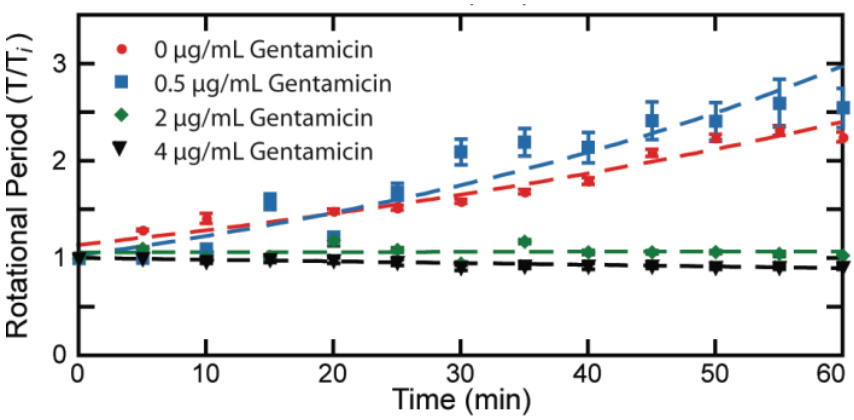

Figure 9: Small population *E. coli* growth curves measured with AMBR biosensor. The MIC, is 1 µg/mL. Bacteria treated with gentamicin concentrations below the MIC continued to grow, whereas bacteria treated with concentrations above the MIC did not show noticeable growth.

Off-the-microscope studies

The ability of the AMBR biosensors to transform femtoliter scale volume changes into frequency variations of orders-of-magnitude-larger magnetic particles is what makes the technology powerful. While most of the AMBR biosensor experiments to date have been conducted on an optical microscope, it is not ideal for automation purposes. The rotation rate of the AMBR sensor can be measured by its vertical displacement over time (see Figure 10) [4], or by focusing a low power laser, which has been done using a simple prototype device without optical microscope [8,9]. A fast Fourier transform (FFT) can be used to decipher the rotation rate of a particle from the periodic raw signal, for example the displacement of the particle or the laser intensity fluctuating due to particle rotation. Using the above mentioned methods, the work is underway to improve AMBR biosensor compatibility with the industry standard 96- and 384-well plates for rapid growth studies such as antimicrobial susceptibility testing (AST) of bacteria, chemotherapy sensitivity and resistance assays (CSRAs) for cancer cells, yeast antifungal testing and research applications.

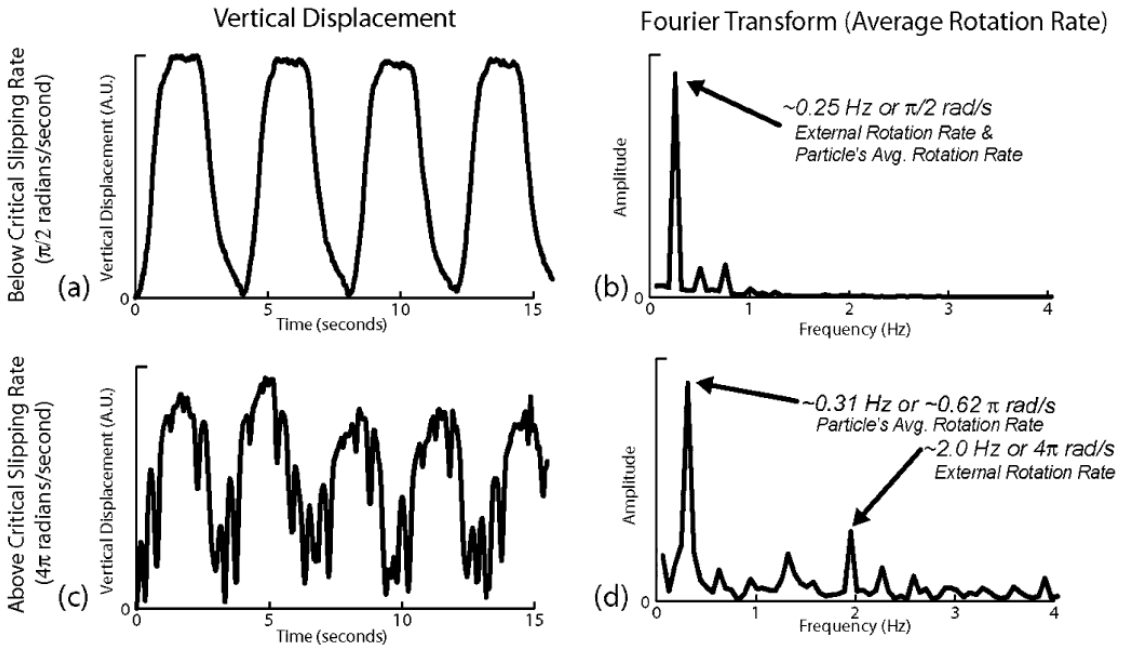

Figure 10: The rotational behavior of a single magnetic particle below (a-b) and above (c-d) the critical driving frequency. From the periodic data, a Fourier transform was taken to determine the average rotation rate, parts b and d. Below the critical driving frequency, part b shows only one main peak, which is a result of the particle being in phase with the external field (with a constant phase lag). At external rates above the critical frequency, part d reveals two main peaks, one that results from the slower net rotation of the particle and one that results from the faster counterclockwise rocking of the magnetic particle.

Cell magneto-rotation (CM) and cancer cell studies

Suspended cells behave differently than adherent cells, which is especially important in predicting the environmental responses of circulating tumor cells (CTCs) and stem cells. However, the growth response of cancer cells in the suspended state is difficult to study due to the lack of existing methods for that purpose. Elbez et al. describe a new method for quantitative, real time monitoring of cell size and morphology, on single live suspended cancer cells, unconfined in three dimensions [7]. The precision is comparable to that of the best optical microscopies, but, in contrast, there is no need for confin-

ing the cell to the imaging plane. The cell magneto-rotation (CM) method is based on nanoparticle induced cell magnetization, where magnetic nanoparticles are attached to the cell or internalized in the cytoplasm. By using a rotating magnetic field, the magnetically labeled cells are actively rotated, and the rotational period is measured in real-time. A change in morphology induces a change in the rotational period of the suspended cell (e.g. a bigger cell rotates slower). Using CM it is possible to monitor cell swelling and death, in real time at the single cell level, see Figure 11. This method could be used for multiplexed real time single cell morphology analysis, with implications for CTC drug sensitivity, drug testing, drug discovery, genomics and three-dimensional culturing [7].

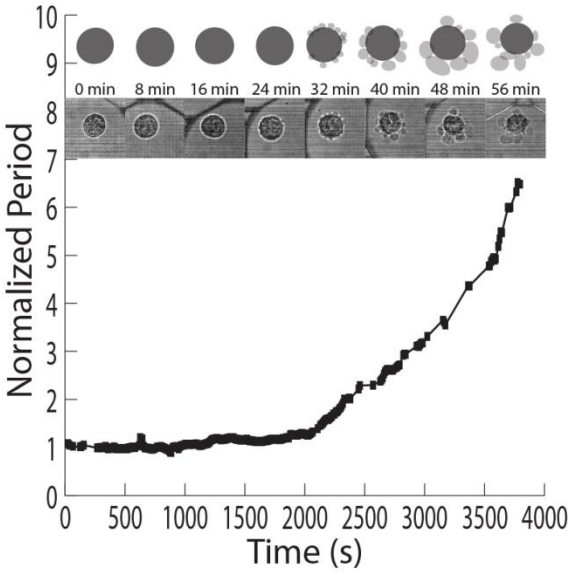

Figure 11: Changes in the rotation period of a single live HeLa cell in 5% Ethanol. The HeLa cell is a human cervical carcinoma cell line, often used as a model system. The bottom pictures show snapshots of the rotated cell at each indicated time, while the schematic pictures on top show the corresponding cell shapes. Dark discs represent the cell cytoplasm and membrane, while grey spots show the vesicles formed at the surface. Note the 550% increase in rotation period due to cell "blebbing".

Label-acquired magneto-rotation (LAM) biosensor

Another type of AMBR based biosensor has been demonstrated, which takes advantage of the fact that the rotation rate depends on the amount of magnetic material present in the particle (see equation 3 and 4) [18]. Instead of measuring volume (and assum-

ing constant magnetic moment), the LAM biosensor measures the magnetic content (and assumes the volume to be constant). Therefore, when a nonmagnetic sphere acquires magnetic moment by specific antigen-antibody interactions, the amount of antigen in the sample is reflected by the acquired magnetic moment and therefore the rotation rate of the particle. See Figure 12 for a schematic of the system. LAM biosensor has been used to detect Thrombin with a limit of detection below 1 nM, where Thrombin was used a model system for relevant detection system.

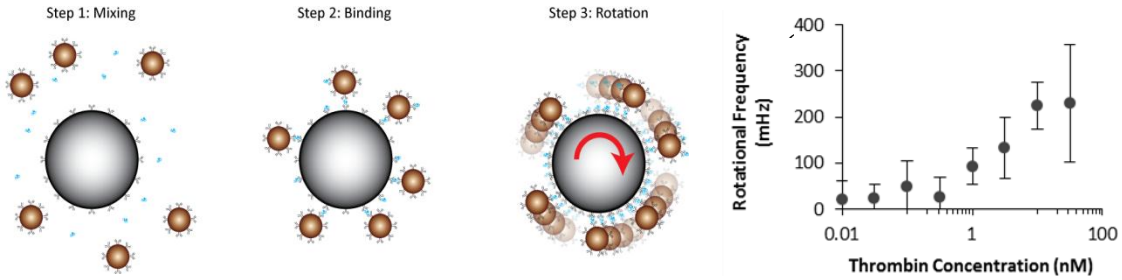

Figure 12: **a**) Schematic illustrating label-acquired magnetorotation. A central 10 μm nonmagnetic sphere and 1 μm superparamagnetic label beads are coated with a sandwich pair of affinity molecules (either antibodies or aptamers) specific to the target, and are then mixed with the target. The target is sandwiched between the central sphere and the label beads, creating a magnetic sandwich complex. The sandwich complex is transferred to a rotating magnetic field, where the rotational frequency of the sandwich complex is a function of the number of attached superparamagnetic label beads (and therefore the concentration of the target as well). In the absence of the target, a sandwich complex is not formed, so the nonmagnetic central sphere does not rotate in the magnetic field. **b**) An example of the application of label-acquired magnetorotation. Thrombin was chosen as a sample analyte and detected using a sandwich aptamer pair.

Magnetically modulated optical nanoprobes

Modulated optical nanoprobes (MOONs) can be nonmagnetic, modulated by Brownian rotation [44], or magnetic, modulated with magnetic fields (Mag-

MOONs)[45,16]. The periodic magnetic modulation of the MagMOONs can be used to separate a weak fluorescent signal from the background fluorescence (Figure 13).

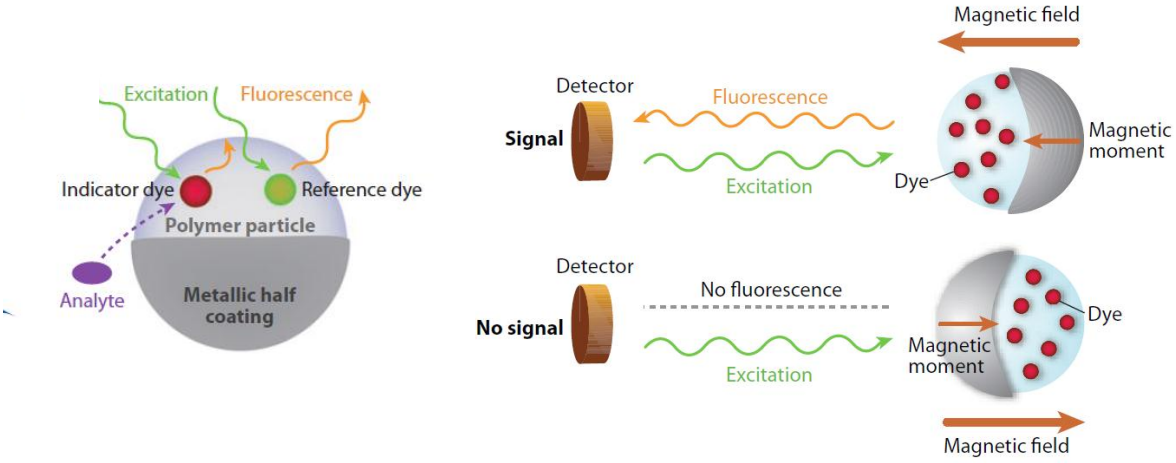

Figure 13**:** (a) Modulated optical nanoprobe sensor. (b) Background-free measurement taken by a magnetically modulated optical nanoprobe (MagMOON). An external magnetic field orients the MagMOON, causing its fluorescent excitation and observed emission to blink on and off as it rotates. Note that the background fluorescence does not blink.

This simple procedure increases the signal-to-background ratio by 3-4 orders of magnitude [45], enabling the use of fluorescent nanoparticle sensors in samples with highly scattering or fluorescent backgrounds. The MOON functionality can be added to any fluorescent nanoparticle sensor by using a vacuum deposition with magnetic or non-magnetic metal as the coating material. The MOONs have also been used for local viscosity measurements by using the AMBR technique [22], which enables simultaneous physical and chemical measurements if fluorescent probes are used.

Outline of the Dissertation

The chapters in this dissertation have either been published in some form or will be submitted. The full references for each publication are:

Chapter I: Kinnunen, P., Hrin, A, McNaughton B. H. and Kopelman R. Asynchronous magnetic bead rotation (AMBR) biosensors and biomedical applications. In J. N. Anker and T. Mefford (Ed.) *Biomedical Applications of Magnetic Particles.* Taylor & Francis. (In Press 2011)

Parts of the chapter also included in U.S. provisional patent application No. 61/474,113 "Magnetic-Label-Acquired Rotation to Measure the Concentration of a Protein or Other Biomarker in Solution" filed on April 11th, 2011.

Chapter II: Kinnunen, P., I. Sinn, B. H. McNaughton, and R. Kopelman. 2010. High frequency asynchronous magnetic bead rotation for improved biosensors. *Applied Physics Letters* 97, no. 22. doi: 10.1063/1.3505492.

Chapter III: Kinnunen, P., I. Sinn, B. H. McNaughton, D. W. Newton, M. A. Burns, and R. Kopelman. 2011. Monitoring the growth of individual bacteria using asynchronous magnetic bead rotation sensors. *Biosensors and Bioelectronics*. doi: 10.1016/j.bios.2010.10.010.

Chapter IV: McNaughton, B. H., P. Kinnunen, R. G. Smith, S. N. Pei, R. Torres-Isea, R. Kopelman, and R. Clarke. 2009. Compact sensor for measuring nonlinear rotational dynamics of driven magnetic microspheres with biomedical applications. *Journal of Magnetism and Magnetic Materials* 321, no. 10 (May): 1648-1652. doi: 10.1016/j.jmmm.2009.02.106.

Chapter V: Kinnunen, P, B. H. McNaughton, T. Albertson, I. Sinn, S. Mofakham, D. Newton, A. Hunt and R. Kopelman. (To be submitted 2011) Self-assembled magnetorotation sensors for bacterial drug resistance.

Parts of the chapter also included in U.S. provisional patent application No. 61/474,123 "Asynchronous Magnetic Bead Rotation Sensing Systems and Methods." filed on April 11th, 2011. And in U.S. provisional patent application No. 61/402,310 "Multi-Well Reader Device, Disposable Card, and Method for Asynchronous Magnetic Bead Rotation Assays."

Appendix A: A literature review by Kinnunen, P. Not published.

Appendix B: Kinnunen, P, D. Youngstrom, B. H. McNaughton and R. Kopelman. Not published.

Appendix C: Kinnunen, P, I. Sinn, B. H. McNaughton and R. Kopelman. Not published.

CHAPTER II:

High frequency AMBR for improved biosensors

Biosensors with increasingly high sensitivity are crucial for probing small scale properties. The Asynchronous Magnetic Bead Rotation (AMBR) sensor is an emerging sensor platform, based on magnetically actuated rotation. Here the frequency dependence of the AMBR sensor's sensitivity is investigated. An asynchronous rotation frequency of 145 Hz is achieved. This increased frequency will allow for a calculated detection limit of as little as a 59 nm change in bead diameter, which is a dramatic improvement over previous AMBR sensors and further enables physical and biomedical applications.

Introduction

Magnetic beads are used in a variety of applications, such as micro mixing [12,46,47], analyte enrichment [48-50], and biosensors [5,51-54]. Immunomagnetic separation and the availability of various magnetic bead biosensors allows for analyte isolation and detection with a single platform. Our current work concentrates on Asynchronous Magnetic Bead Rotation (AMBR) sensors, which have the capability of measuring changes in the sample over time, whereas much of the past work with magnetic bead biosensors has concentrated on analyte detection. AMBR has been previously utilized for

sequential detection of individual bacterial cells in fluid [5]. Only recently have fluidic environments been incorporated into other high resolution sensing techniques, such as micromechanical oscillators [55], allowing for real time studies of live cells [56]. Higher frequency asynchronous magnetic bead rotation allows more averaging, higher resolution and higher bandwidth studies, which will allow applications such as (1) real time single bacterium growth monitoring with sub-diffraction limited sensitivity and (2) single virus detection, both in their given fluid environment.

Theory of high frequency AMBR

In a rotating magnetic field, the motion of a ferromagnetic bead becomes asynchronous with the field above a critical driving frequency, Ω_c. The rotation in the synchronous regime (i.e. below the critical driving frequency) has been used for a variety of applications [57,58]. The AMBR approach concentrates on the asynchronous regime. Recall from the first chapter that the critical driving frequency for a ferromagnetic bead is a function of the permanent magnetic moment of the bead, m, the magnetic field strength, B, the shape factor, κ (which is 6 for a sphere), the kinematic viscosity, η, and the volume of the bead, V

$$\Omega_c = \frac{mB}{\kappa\eta V}. \tag{13}$$

And above the critical driving frequency, the (asynchronous) rotation frequency of the bead, $\langle\dot{\theta}\rangle$, is described by equation (3) given again below:

$$\langle \dot{\theta} \rangle = \Omega - \sqrt{\Omega^2 - \Omega_c^2}\,, \tag{14}$$

where Ω is the driving frequency. AMBR can also be performed with superparamagnetic beads; however, we limit our theoretical discussion here to ferromagnetic beads.

To date, the reported rotational frequencies for AMBR sensors have been between 0.2 and 29 Hz [4,5,20,22,28,35,37,59,60], as summarized in Table I. Current AMBR applications, such as micro mixing, pathogen detection and growth studies could all benefit from higher rotational frequencies. We therefore investigate the AMBR probes' sensitivity, with respect to the bead rotation frequency, and demonstrate a system with a 49.15 Hz asynchronous rotation frequency, and achieve a 145 Hz critical frequency. The demonstrated system consists of a ferromagnetic bead driven with a 1 mT magnetic field in water. The experimental data is accurately described using ferromagnetic particle theory (Equation 14), with no observed contribution of superparamagnetic origin [4,37].

Table I: Reported critical frequencies of magnetically actuated asynchronously rotating systems in the literature. We designate $\langle \dot{\theta} \rangle_{\max}$ as the approximate maximal rotational frequency of the driven system.

$\langle \dot{\theta} \rangle_{\max}$ (Hz)	Driven system	Author
159	Elongated magnetic particles	Tierno[a]
145	Magnetic half coated beads	Kinnunen[b]
29	Two bound magnetic particles	Ranzoni[c]
12	Magnetic microparticles	Janssen[d]
10	Magnetic carbon nanotubes	Korneva[e]
6.3	Magnetic hole systems	Helgesen[f]
2.4	Ferromagnetic beads	McNaughton[g]
1.08	Barium ferrite particles	McNaughton[h]
0.95	Magnetic microspheres	McNaughton[i]
0.2	Ferromagnetic beads	McNaughton[j]

[a]Reference [28]	[f]Reference [59]
[b]Reference [9]	[g]Reference [5]
[c]Reference [60]	[h]Reference [4]
[d]Reference [37]	[i]Reference [22]
[e] Reference [35]	[j]Reference [8]

Materials and Methods

Magnetic beads were prepared using a previously reported method [61]. A mono-layer of 6.7 μm diameter polystyrene particles (Spherotech TP-60-5) was coated with a 340 nm thick Nickel layer and magnetized in a 200 mT magnetic field, perpendicular to the surface. This process results in half-coated beads, where one side is nickel and the other hemisphere is polystyrene. The beads were resuspended in deionized and filtered water, with 0.5 % of sodium dodecyl sulfate. Nunc, LiveCell Array slides (Thermo Fisher Scientific, Rochester) were used to keep each bead from significant translational move-ment during the experiment. The beads were placed in a rotating magnetic field where the rotation was analyzed; see Figure 14 for a schematic of the system. A set of two custom built perpendicular Helmholtz coils was used to generate a rotating magnetic field with magnitudes of 0.25 mT to 1 mT, at frequencies 1 Hz to 1 kHz; Figure 14b.

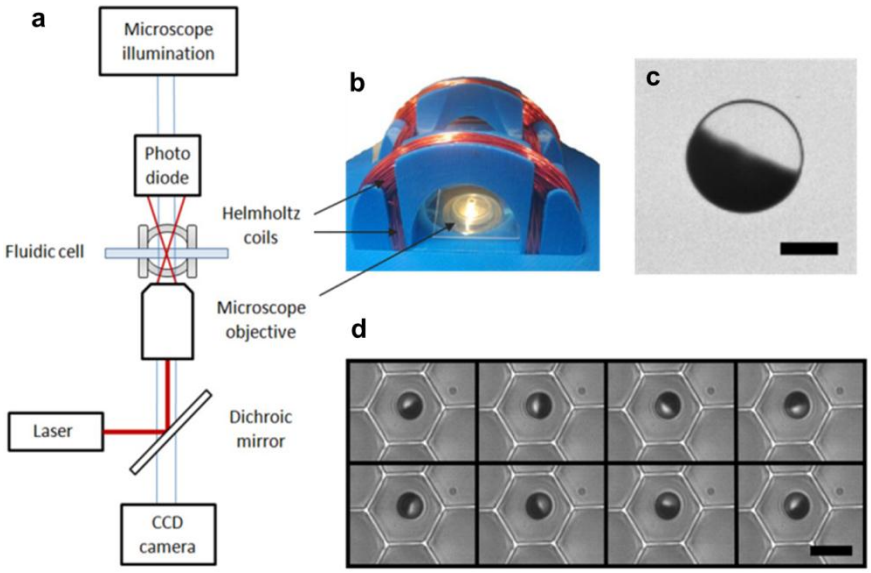

Figure 14: (a) Schematic representation of the laser and microscope setup in which a low power laser, in conjunction with a dichroic mirror, a microscope objective and a photodiode, was used to measure the rotation rate of a single magnetic bead. A digital camera can be used to simultaneously capture a video of the rotating system. (b) Custom designed Helmholtz coils were used to create a rotating magnetic field in the imaging plane. (c) An optical microscope image of a half coated 10 µm bead (300 nm Nickel coating) with a 5 µm scale bar. (d) Image sequence of a 6.7 µm bead rotating synchronously in the LiveCell Array in a 10 Hz field. The time between each frame is 14 ms and the scale bar is 10 µm.

The rotational frequencies of the magnetic beads, shown in Figure 15, were measured by focusing a low power laser (633 nm, 2.5 mW) on the bead of interest and analyzing the modulation frequency of the deflected light; the light is modulated once during every bead rotation due to the nickel half coating. The light modulation could be measured by placing a 13 mm^2 photodetector above the sample, (Thorlabs, PDA36A) ~100 mm away and a few centimeters off-center of the laser beam exiting the sample. This was achieved by using a dichroic mirror that passes all wavelengths but that of the laser (Figure 14a). Measurements were taken on an inverted microscope (Olympus, IX 71) with a photodetector, a data acquisition board (National Instruments, NI PCI-6221) and

analyzed with a Fast Fourier Transform (FFT) routine, implemented in a LabView (National Instruments) program. For Figure 16, the rotation rates were determined using a digital camera (Basler, piA640-210gm); the videos were taken at 383 frames per second, and analyzed with ImageJ software by plotting a region of interest (ROI) intensity over time and applying a FFT with a 512 point Dirichlet window (512 points equals 1.3 seconds).

Results and Discussion

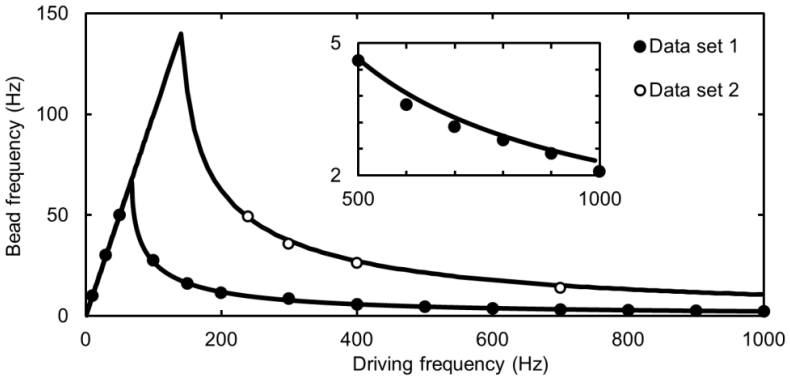

Figure 15: The bead rotation frequency at varying driving frequencies for two 6.7 μm magnetic beads with rotating magnetic field strengths of 0.5 mT and 1 mT for data sets 1 and 2, respectively. The data is fitted with a single parameter least squares method to the theory of a ferromagnetic bead in a rotating magnetic field (Equation 14). Inset: Data set 1 zoomed in at the high driving frequency region, so as to demonstrate the quality of the fit.

In this letter, the sensitivity of the AMBR sensor, S, is defined as the smallest detectable change in the system's hydrodynamic radius, Δr, and it is governed by the uncertainty in the bead frequency measurement, $\Delta\langle\dot{\theta}\rangle$. The partial derivative method can

be used to investigate how the uncertainty in the bead frequency $\Delta\langle\dot{\theta}\rangle$ affects the uncertainty in the bead radius

$$\Delta r = \left|\frac{\partial r}{\partial\langle\dot{\theta}\rangle}\right| \times \Delta\langle\dot{\theta}\rangle . \tag{15}$$

The radius r can be solved as a function of the bead frequency $\langle\dot{\theta}\rangle$, using equations (13) and (14) and assuming a spherical bead. The partial derivative can be carried out and if a constant ratio $\langle\dot{\theta}\rangle/\Omega = 1/5$ is assumed, one obtains

$$\frac{\Delta r}{r} = \frac{1}{3} \times \frac{\Delta\langle\dot{\theta}\rangle}{\langle\dot{\theta}\rangle} . \tag{16}$$

Therefore, the relative uncertainty in bead radius is proportional to the relative measurement uncertainty and has no explicit frequency dependence. The sensitivity of the system is therefore

$$S = \frac{r}{3} \times \frac{\Delta\langle\dot{\theta}\rangle}{\langle\dot{\theta}\rangle} . \tag{17}$$

In order to measure the uncertainty of the bead rotation measurement, a 6.7 μm diameter magnetic bead AMBR sensor was driven with a 400 Hz, 1 mT rotating magnetic field and was continuously measured for 37 seconds. The data are shown in Figure 16. The average rotation period was 25.4 Hz, with a 0.7 Hz standard deviation. Using these values and Equation (17) to calculate the sensitivity, the AMBR sensor was found to be sensitive to a 59 nm bead diameter change, which corresponds to a 4 femtoliter volume

change. We anticipate that this sensitivity will allow for applications such as (i) real time single bacterium growth monitoring with sub-diffraction limited sensitivity and (ii) single virus detection, both in their given fluid environment.

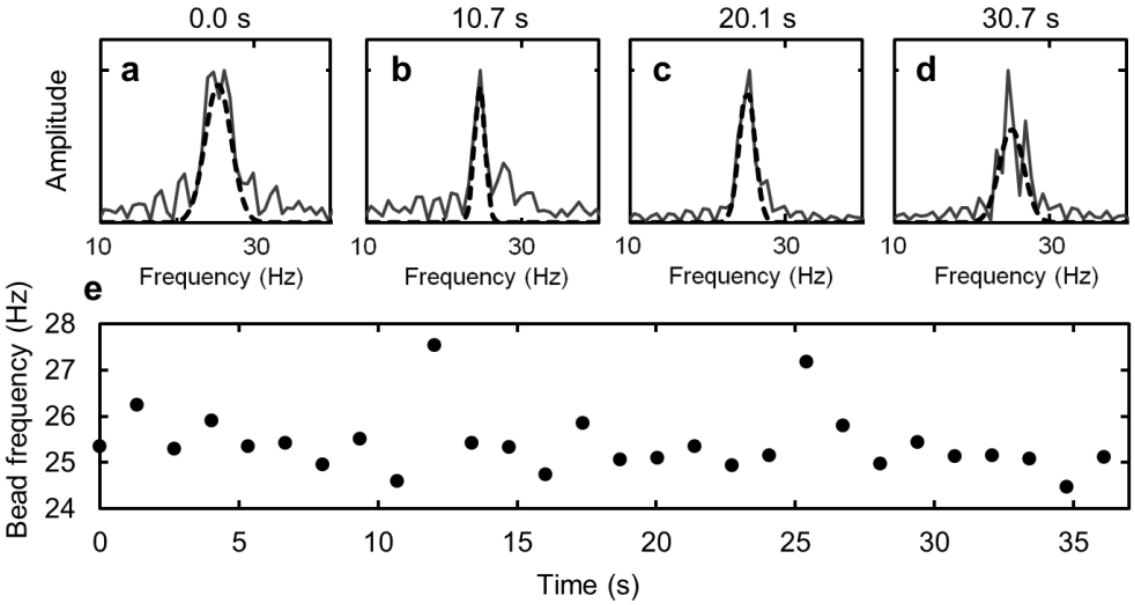

Figure 16: The AMBR sensor signal in time. (a-d) Fast Fourier Transform plots of rotation data, at time 0 s, 10.7 s, 20.1 s and 30.7 s. (e) The rotational period of the AMBR sensor in time, as measured with the Fourier analysis, examples of which are shown in parts a-d. The average of the bead frequency is 25.4 ± 0.7 Hz. The AMBR sensor is a 6.7 μm magnetic bead in 31 ^{o}C water.

To investigate the feasibility of the presented AMBR system for micro mixing applications, we calculated the maximum Reynolds number of the system [22] $\mathrm{Re}_{\max} \approx 1 \times 10^{-2}$. Although this value is low for micro mixing applications, it is be possible to achieve significantly higher Reynolds number values by increasing the magnetic field strength, bead size, amount of magnetic material, and/or by using a material with higher magnetic moment. For systems with a constant ratio of hydrodynamic volume to magnetic content volume, the critical rotational frequency remains constant for all sized

particles. This suggests that Reynolds numbers of ~10 can be achieved with an order of magnitude larger bead having a nickel coating amounting to 5 % of its diameter. Increased rotational frequencies of the magnetic beads reported in this letter were achieved by fabricating custom magnetic beads by thermally evaporating nickel onto nonmagnetic microparticles. Equation (14) was used to calculate the magnetic moment of the individual beads [22] with a 145 Hz critical frequency, 6.7 μm diameter, 1 mT magnetic field, 1 mPas dynamic viscosity and a shape factor of 6 yielding $m \approx 8.6 \times 10^{-13} Am^2$. Applications other than micromixing could be possible by the use of high frequency rotation, such as drag based binding affinity measurements. For example, the tension exerted onto a 10 nm long molecular tether attaching a 1 μm bead to the equator of a 6.7 μm ferromagnetic bead rotating synchronously at 145 Hz was estimated to be on the order of 1 pN; this value is large enough to break non-specific bond interactions [51].

In summary, we demonstrated high frequency AMBR measurements with up to 145 Hz critical driving frequency and calculated the resulting sensitivity of 59 nm change in the bead diameter, corresponding to a 4 femtoliter volume change. This sensitivity could allow for improved single bacterium growth monitoring and single virus detection. Furthermore, the high frequency rotation regime might also be used for applications such as micromixing and binding affinity measurements.

CHAPTER III:

Monitoring the growth of individual bacteria using asynchronous magnetic bead rotation sensors

Introduction

Continuous growth of individual bacteria has been previously studied by direct observation using optical imaging. However, optical microscopy studies are inherently diffraction limited and limited in the number of individual cells that can be continuously monitored. Here we report on the use of the asynchronous magnetic bead rotation (AMBR) sensor, which is not diffraction limited. The AMBR sensor allows for the measurement of nanoscale growth dynamics of individual bacterial cells, over multiple generations. This torque-based magnetic bead sensor monitors variations in drag caused by the attachment and growth of a single bacterial cell. In this manner, we observed the growth and division of individual *E. coli* bacteria, with 80 nanometer sensitivity to the cell length. Over the life cycle of a cell we observed up to 300 % increase in the rotational period of the biosensor due to increased cell volume. In addition, we observed single bacterial cell growth response to antibiotics. This work demonstrates a non-microscopy

based approach for monitoring individual cell growth dynamics, including cell elongation, generation time, lag time, and division, as well as their sensitivity to antibiotics.

Optical microscopy is currently the most widely used tool for studying single cell behavior, as it offers the ability to measure the elongation of individual bacteria over multiple generations [39-41]. However, the spatial resolution of far-field optical microscopy techniques is limited by the diffraction of light. High sensitivity tools that have proven useful for single cell analysis include scanning probe techniques [42] and cantilevers [43], but studies spanning multiple generations of individual cells have not yet been demonstrated with these techniques. We note that high resolution techniques, such as electron microscopy and cantilevers are optimal in air, rather than in water. Here we present a high-resolution sensing method that works optimally in aqueous environments [22].

In this manuscript, we implement the asynchronous magnetic bead rotation (AMBR) method to measure the nanogrowth of individual bacterial cells. AMBR sensors, as reported by our lab, have previously been used for a variety of applications [4,5,20,22]. The rotational dynamics of magnetic objects rotating asynchronously with the driving magnetic field have also been used for a other applications and investigations. One of the first investigations was a system consisting of a ferrofluid and a pair of non-magnetic rotating spheres called “magnetic holes” [32,59]. Similar magnetic rotational studies have been used for the characterization of magnetic carbon nanotubes [35], magnetotactic bacteria [62], traveling wave magnetophoresis [15,63], micro mixing [12,64], and artificial microscopic swimmers and microdrills [10,65]. Additionally, nonmagnetic

systems that undergo asynchronous rotation have been used for the rotation of glass nanorods in fluid [29]. The presented AMBR method enables the growth of a single bacterium to be measured throughout its life cycle and over sequential generations. Indeed, we show that the elongation of individual *E. coli* bacterial cells can be observed with 80 nm sensitivity in cell length. This high-sensitivity, prolonged monitoring, single cell analysis technique could be useful in population heterogeneity studies, and could radically shorten the test time for identification (ID) and antimicrobial susceptibility testing (AST) of microorganisms.

As mentioned, these single cell studies employ the AMBR method [4,5,20,22],

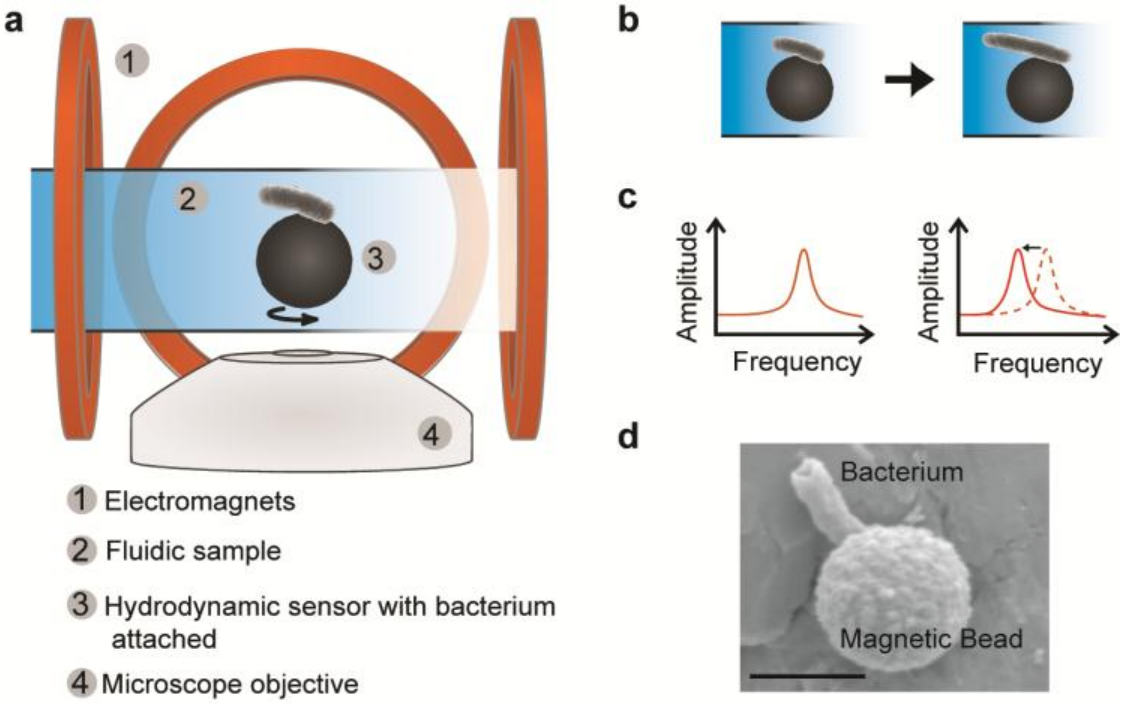

Figure 17: The concept of measuring single cell elongation using the asynchronous magnetic bead rotation (AMBR) method. (a) A schematic representation of the AMBR sensor on a microscope. (b) Cell elongation (schematic). (c) Schematic illustrating of how the rotational period change is observed as a peak shift in the FFT spectrum (i.e. the elongation of the attached bacterium can be measured by observing the change in the rotational period of the sensor-bacterium complex, which is caused by the increase in the system's effective volume). (d) Scanning electron microscopy image of a magnetic bead system, in which a single E. coli cell is attached to a 2.8 µm magnetic bead. The scale bar is 2 µm.

which is based on the torque exerted on a magnetic bead in the presence of a rotating magnetic field. At sufficiently high rotating field frequencies, the magnetic bead rotates asynchronously with the magnetic field [4,62] and in the case of a superparamagnetic bead the rotational period, T, is proportional to the effective volume of the rotating body, $T \propto V_{eff}$. In the asynchronous rotational regime, the effective volume is defined as $V_{eff} = \kappa V$, where κ is the Einstein shape factor (6 for a sphere, and higher for other shapes). For a complete derivation, see **Theoretical derivation** section (below). Therefore, by monitoring the rotational period of the magnetic bead, it is possible to detect single bacterium binding events [5] and, as demonstrated in this manuscript, measure single bacterial cell growth on the nanometer scale. When a single cell attaches to a magnetic bead, or grows, the effective volume of the bead complex increases; this process can be monitored by measuring changes in the bead's rotational period. The *E. coli* are assumed to grow only in length [41], with a constant diameter; thus changes in the rotational period of the bead correspond to bacterial elongation. A schematic of this is shown in Figure 17(a-c). Within this manuscript, the sensitivity is defined as the smallest detectable change in the sensor or its environment.

Materials and methods

Theoretical derivation

The torque exerted on a magnetic bead in a magnetic field can be expressed by

$$\boldsymbol{\tau}_{mag} = \mathbf{m} \times \mathbf{B} = \left(\mathbf{m}_{perm} + \mathbf{m}_{ind} \right) \times \mathbf{B}, \tag{18}$$

where $\boldsymbol{\tau}_{mag}$ is the total magnetic torque due to the induced magnetic moment $\mathbf{m}_{ind}$ and permanent magnetic moment $\mathbf{m}_{perm}$, in a magnetic field $\mathbf{B}$. In a time varying magnetic field, the induced magnetic moment is not necessarily parallel to the magnetic field, and therefore can contribute to the torque. By use of previously described equations for asynchronous rotation, arising from magnetic torque [4,37,62], the total magnetic torque in a rotating magnetic field can be expressed by

$$\boldsymbol{\tau}_{mag} = \left[\mathbf{m}_{perm} + \left(\chi' + i\chi''\right)V_m\mathbf{B}\right]\times\mathbf{B} = m_{perm}B\sin\left(\Omega t-\theta\right)\hat{\mathbf{e}} + \chi'' V_m B^2 \mu_0^{-1}\hat{\mathbf{e}}, \qquad (19)$$

where χ' is the real part and χ'' is the imaginary part of the magnetic susceptibility, Ω is the driving frequency, V_m is the magnetic content volume, μ_0 the permeability of free space, and $\hat{\mathbf{e}}$ is a unit vector. The real part of the susceptibility, χ', does not contribute to the cross product in Equation (19), as it remains parallel with the magnetic field. The first term on the right hand side of Equation (19) corresponds to the permanent magnetic moment, and the second term corresponds to the induced (superparamagnetic) moment. In the experiments, we implement a 500 Hz driving field while the critical frequency of the system, Ω_c, is on the order of 1Hz. As a result, the superparamagnetic torque dominates and the first term in Equation (19) can be neglected ($\Omega >> \Omega_c$). This allows for Equation (18) to be simplified to

$$\boldsymbol{\tau}_{mag} = \mathbf{m}_{ind}\times\mathbf{B}, \qquad (20)$$

leading to

$$\boldsymbol{\tau}_{mag} = \chi'' V_m \frac{B^2}{\mu_0} \hat{\mathbf{e}} . \tag{21}$$

Neglecting both inertial forces (where drag forces dominate) and Brownian rotation forces (where magnetic torque dominates) the torque of a rotating body in a viscous fluid [4,22,62] can be expressed by:

$$\boldsymbol{\tau}_{drag} = -\boldsymbol{\tau}_{mag} = -\kappa \eta V \dot{\theta} \hat{\mathbf{e}}, \tag{22}$$

where κ is the Einstein shape factor, η is the dynamic viscosity of the surrounding fluid, V is the total volume of the rotating body, and θ is the angular orientation ($\dot{\theta}$ is the rotational rate of the object, in radians/s). The rotational rate of the object can be solved by combining Equations 21 and 22, which yields

$$\dot{\theta} = \frac{\chi'' V_m B^2}{\kappa \eta V \mu_0} . \tag{23}$$

At a constant temperature and a constant rotating magnetic field, the imaginary susceptibility χ'', magnetic content volume V_m, magnetic field strength B, and the dynamic viscosity η, remain constant. Under these conditions, the rotation rate of the particle is primarily a function of the effective volume

$$\dot{\theta} \propto \frac{1}{V_{eff}}, \tag{24}$$

The rotational period of the particle, *T*, can be written in terms of the rotational rate, $\dot{\theta}$, as $T = 2\pi/\dot{\theta}$, which yields the basis of the superparamagnetic AMBR sensor, namely Equation (25):

$$T \propto V_{eff} . \tag{25}$$

Notably, a similar equation has been reported for the measurement of the Brownian relaxation peak of magnetic particles as measured with AC susceptometry [53]. However, the AMBR method implements constant magnitude rotating magnetic fields and does not use varying magnitude non-rotating fields as is done with AC susceptometers. Thus, Equation (25) does not describe the location of the Brownian relaxation peak. Instead, Equation (25) describes how the real-time rotational period of a magnetic particle relates to the effective volume of the particle, when driven at a single frequency.

Cell culture and attachment methods

Uropathogenic *E. coli* bacteria (obtained from the Clinical Microbiology Laboratory, University of Michigan Hospital) were grown on Mueller-Hinton agar plates (BBL) at 37 ^{o}C for 12 to 18 hours. The bacteria were then suspended in 2.2 % Mueller Hinton II (MH) broth (Teknova) to the approximate concentration of 1.5×10^{8} CFU/mL (e.g. a 0.5 McFarland Standard value). Anti-*E. coli* (Abcam, ab20640-1) functionalized magnetic particles (Invitrogen M-280) were introduced to the bacteria solution (to yield 10^{6} beads/mL concentration). The sample was incubated, with 175 rpm shaking at 37 ^{o}C, for another 1.5 hours. Before rotational data were obtained, the beads with attached bacteria were isolated using a magnetic separator (PickPen 1-M) and re-suspended into a solution

containing MH broth with 1 % Pluronic F-68 [66] (MP Biochemicals) and 0.1 % BSA (Thermo Scientific). All experiments were conducted at room temperature. The minimum inhibitory concentration (MIC) of the *E. coli* was measured as 8 µg/mL ampicillin, as determined by conventional broth microdilution methods.

Experimental setup and measurement conditions

Isolated bead-bacteria complexes were placed in a rotating magnetic field on an inverted optical microscope (Olympus IX71, 100x/1.3 oil) and 1 minute videos were taken at 5 minutes intervals at 16 fps using a digital camera (Basler, piA640-210gm), see Figure 18. Videos were analyzed using ImageJ software [67] by plotting the "z-axis profile" of an area of interest next to the rotating particle; this yields an intensity profile that reflects the rotational frequency of the bead-bacterium complex [4]. The intensity plot was analyzed by applying a Fast Fourier Transform (FFT) in Matlab (The MathWorks, 2009), and the frequency of the highest amplitude FFT peak indicate the rotational rate of the particle (see Figure 17). Occasionally, the highest amplitude FFT peak did not correspond to the observed rotational frequency of the particle, and instead was twice the observed rotational rate. The peaks were fitted with a Gaussian function in order to determine the peak position and width. The rotating magnetic field was generated with a custom Labview (National Instruments) program and Data Acquisition Board (NI PCI-6221) in conjunction with an amplifier and a custom made pair of air core Helmholtz coils. The magnetic field frequency used to rotate the magnetic beads was 500 Hz with a 0.9 mT

magnitude, which was measured with a 3-axis magnetic field probe (Senis Gmbh, C-H3A-2m).

Experimental errors

The error in determining the rotational period was designated as the FFT peak width (FWHM) of the amplitude signal (Figure 18 and Figure 19). Fixed cells (*E. coli* suspended in 1 % Glutaraldehyde for 30 minutes) were measured over 120 minutes, yielding a 6.0 % CV in the rotational response of the sensor. Fluctuations in the rotational response of a single AMBR probe, with no bacteria present, were under 10 % after 20 hours, showing long term stability in the rotational period. Bacterial length measurements were performed with a bright field microscope and a 100X oil immersion objective. The theoretical diffraction limit is estimated to be $\lambda/(2N.A.) \approx 700\,\text{nm}/2.6 \approx 270\,\text{nm}$, which we assumed to be our error in the bacterium length measurements on the microscope. To determine the bacterial cell length, intensity profiles were taken across the length of the bacterium, with ImageJ software.

Results and discussion

We demonstrated the sensitivity of the AMBR method by measuring the growth and division of a single *E. coli* cell throughout its life cycle and over multiple generations (Figure 18). Bacterial cells were attached to 2.8 μm diameter magnetic beads coated with specific antibodies. After immunomagnetic separation, individual cell growth and response to antibiotics were observed by using the AMBR method. Measurements per-

formed on an inverted bright-field microscope allowed for visualization of bacterial elongation and division, Figure 18b, and quantification of the resulting changes in the rotational period of the sensor, Figure 18c (normalized data). Over the first cell division cycle, the rotational period of the AMBR sensor changed from (0.8 ± 0.03) s to (3.2 ± 0.2) s, which corresponds to a 300 % increase in the rotational period. Similarly, over the second and third cell divisions, the periods changed from (1.0 ± 0.1) s to (6.2 ± 0.4) s (520 %) and from (2.3 ± 0.2) s to (5.8 ± 0.3) s (150 %), respectively. These dramatic changes in the rotational period are governed by the volumetric changes of the attached bacteria. The significant abrupt reduction in rotational period at time 104 minutes (e.g. a factor of 2.1 ± 0.3) is exactly, time wise, correlated to cell division as observed on the optical microscope. Furthermore, the rotation of the bead did not lead to the detachment of any bacteria from the bead, thus enabling studies spanning multiple generations. Detachment was only observed as a result of cell division. Upon division, the daughter cell either re-bound to the sensor or detached itself from the sensor and remained free-floating in the medium. For example, a division event that did not result in detachment can be seen in Figure 18c at 104 minutes; and a division with detachment occurred at 177 minutes. In the case where the daughter cell remained bound to the sensor, an abrupt decrease in the rotational period was observed as the bacteria reoriented itself on the bead and lowered the effective volume (by reducing the shape factor).

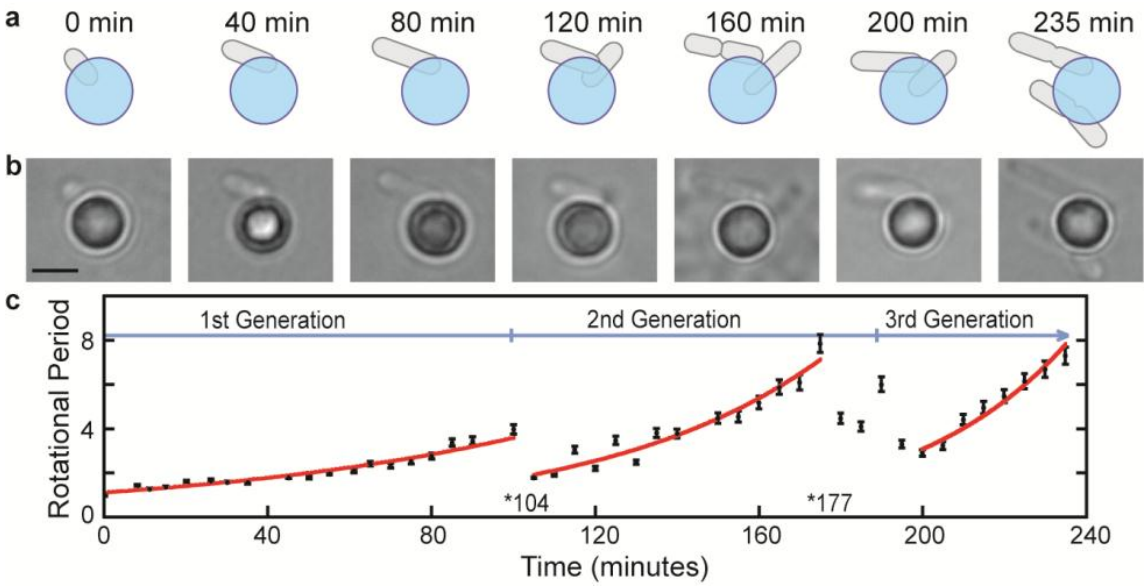

Figure 18: Growth and division of a single *E. coli* bacterium, measured with an AMBR sensor and observed with an optical microscope. (**a**) Schematic figures and (**b**) 100X oil immersion optical microscopy images of the magnetic particle sensor with initially a single bacterium attached and subsequent cell divisions. The scale bar is 2 μm. (**c**) Cell growth and division as observed with the AMBR sensor. After a period of growth, the first cell division is observed at 104 minutes and again at 177 and 199 minutes. The error bars correspond to the measurement error in the rotational period and the exponential fits are a guide to the eye. Data is normalized to 1 at time zero.

Changes in the rotational period of the AMBR sensor are indeed due to bacterial growth, as there were no significant rotational period changes observed when bacteria were not present or when fixated *E. coli* cells were attached **(**Figure 19a). A comparison shows that the rotational period of the AMBR sensor and the optical microscopy measurements of the cell elongation were in good agreement **(**Figure 19b) and consistent with the derived linear relationship. To estimate the sensitivity of the AMBR sensor in response to cell elongation, the rotational period of the sensor (ie. the sensor signal) was correlated to the cell length as measured by optical microscopy. The sensitivity depends on the orientation of the bacterium, and is therefore case dependent. An example of the

relationship between the rotational period of the AMBR sensor and the attached bacterium is shown in Figure 19b, where the error in measuring the AMBR rotational period was estimated to correspond to (80 ± 38) nm change in bacterium length. The fit in Figure 19b was used as the relationship between the rotational period and the bacterium length. The error in optical cell length measurements was approximately 270 nm with our microscope setup, see **Experimental errors** section for the calculation. We measured the rotational period from a series of images, obtained with an optical microscope; however, with the AMBR method, rotation can also be observed without a microscope, by just using a combination of a low power laser and a photodiode [20]. The authors note that the AMBR method is based on the rotational period of the magnetic particle and as a result is unaffected by the optical resolution.

To demonstrate the use of an AMBR sensor for observing single cell response to different environmental conditions, the response of individual *E. coli* cells to two concentrations of antibiotics was measured. The *E. coli* growth, in the presence of a low concentration of antibiotics (0.5 μg/mL ampicillin), and growth inhibition, in the presence of a high antibiotic concentration (8 μg/mL ampicillin), were observed using the AMBR sensor. These growth trends were again confirmed with optical microscopy (Figure 19). The observed response of the individual cells to the specified concentration of ampicillin should not be generalized to the whole population, since different cells within the same population may respond differently at the same concentration of antibiotics, due to the heterogeneity within the bacterial population. Nevertheless, a drastic difference is seen between the normal growth pattern below the antibiotics MIC value and the “no growth”

pattern at the MIC. The ultimate sensitivity of this method depends on the orientation of the attached bacterium and the axis of rotation of the bacterium-sensor complex. However, irrespective of this sensitivity limitation, the method can be used to clearly distinguish between growth and no growth of individual bacteria, as shown in Figure 19c, where growth was arrested by a sufficient concentration of ampicillin. This validates the AMBR sensor as a useful tool for sensitively observing the response of individual *E. coli* cells to environmental effects, in particular to antibiotics, within only minutes.

In addition to using the method to study single cell response to environmental conditions, it is envisioned that this method could ultimately also be used for drug discovery research and for rapid antimicrobial susceptibility testing (AST) in clinical settings. The current clinical standard in AST is based on turbidity measurements of bacteria populations, leading to an approximately 24 hour instrument time when performed on pure cultures [1]. Since the AMBR sensor measures the response of individual bacterial cells instead of changes in the entire population, multiplexing this technique could dramatically reduce AST times. Furthermore, integration with a high-throughput microfluidic technology should enable studies on growth dynamics of individual bacteria, and on their susceptibility to environmental factors such as nutrients, temperature, pH and salt levels, as well as to the introduction of antimicrobial agents.

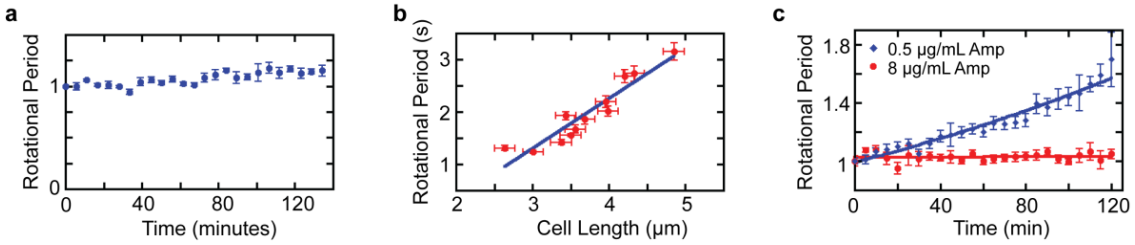

Figure 19: AMBR sensor measurements of elongation, compared with microscope observations, and the effect of antibiotics on cell elongation. (**a**) Fixated E. coli bacterium control data; normalized rotational period of an AMBR sensor with a fixated E. coli attached. (**b**) The rotational period of the AMBR sensor vs. the bacterium length measured from microscopy images, using image analysis. The error bars in the microscope measurement data are 270 nm. The error in the rotational period of the AMBR sensor is explained in the **Experimental errors** section. (**c**) The response of two individual *E. coli* bacteria from the same culture (data normalized to 1 at time zero) in the presence of 0.5 and 8 μg/mL ampicillin, i.e. well below the MIC (growth) and at MIC (no growth), respectively, measured with the AMBR.

Conclusions

The growth of individual *E. coli* bacteria over multiple generations and the effect of antibiotics were measured, at the nanometer scale, using an AMBR sensor. The AMBR biosensor was observed to respond to changes of as little as 80 nm in length of single *E. coli* cells. The sensor was also demonstrated to monitor growth over the entire life cycle of the cells. Furthermore, measurement of the response of individual *E. coli* cells to 0.5 μg/mL and 8 μg/mL concentrations of the antibiotic ampicillin demonstrate a drastic differentiation from "growth" to "no growth". Finally, while the demonstrated AMBR sensor has been optimized for bacteria, preliminary work has extended the method to studies on other individual cells, such as yeast and cancer cells.

CHAPTER IV:

Compact sensor for measuring nonlinear rotational dynamics of driven magnetic microspheres with biomedical applications

Introduction

The linear-to-nonlinear rotational dynamics of magnetic particles have been emerging as both an interesting tool for studying nonlinear dynamics and for biomedical applications such as bacterial detection and growth monitoring [5]. Traditionally, experiments utilize standard microscopy and image analysis techniques to monitor and measure the rotation rate of magnetic and nonmagnetic particles. In the context of potential applications, there remains a need for a more elegant method to measure the rotational dynamics of these particles.

In 1990, the seminal experimental and theoretical work of Helgesen et al. detailed the rotational dynamics of a pair of magnetic holes (non-magnetic microspheres in a ferrofluid), in which *nonlinear* behavior was observed at sufficiently high external magnetic field rotation rates [59]. Many groups followed this work, with various nonlinear rotation studies of small scale systems. For example, Shelton and coworkers used angular momentum from polarized light to torque a glass nanorod [29]. They theorized and experi-

mentally verified that the average rotation rate of the glass rod had a nonlinear dependence on the rotation rate of the polarized light and showed that the nonlinear rotation rate is dependent on the optical torque and fluidic drag of the system. The nonlinear rotation rate of magnetic microspheres has a similar dependence on drag as a torqued glass nanorod. Indeed, Biswal and Gast showed that chains of paramagnetic microspheres are governed by similar rotational dynamics [12].

Korneva and coworkers were among the first to apply the nonlinear rotation rate to measure a physical value. They used this type of rotational behavior to estimate the magnetic moment of carbon nanotubes filled with magnetic nanoparticles [35]. Yellen and colleagues developed a new method of magnetophoresis, based on the principles of asynchronous rotation [15]. Recently, theoretical treatment on single magnetic particle systems have been developed and demonstrated [4,62], but previous studies did not focus on applications of such systems. While many systems have been shown to exhibit nonlinear rotational dynamics, no studies considered single cell detection and growth monitoring applications. To fill this research gap, our group of investigators have studied the nonlinear rotation of magnetic microparticles and explored a number of applications, including single bacterial cell detection [4,5,22]. Here, we describe an important new step in this work, namely the development of a method and device to accurately monitor magnetic particle rotation in a stand-alone configuration.

The orientation and rotation rate of magnetic particles can be measured on account of their physical and optical asymmetries. Nonlinear rotation occurs at high frequencies when the phase-lag between an external rotating magnetic field and the perma-

nent dipole of an aligning magnetic particle exceeds π/2. After this point, the magnetic particle cannot overcome the viscous drag (to remain phase-locked with the external field's rotational frequency) and thus "slips", rotating asynchronously (nonlinear rotational regime) with the driving field. In this case, the average rotational frequency of the magnetic particle has a lower value than that of the driving field. The average particle-rotation-rate, $\langle \dot{\theta} \rangle$, is given by

$$\langle \dot{\theta} \rangle = \begin{cases} \Omega, & \Omega < \Omega_c \\ \Omega - \sqrt{\Omega^2 - \Omega_c^2}, & \Omega \geq \Omega_c \end{cases}, \tag{26}$$

where Ω is the rotational rate of the external field and Ω_c is the critical frequency at which the particle motion changes from being synchronous with the field, to being asynchronous [68,62]. This point of criticality is given by

$$\Omega_c = \frac{mB}{\kappa \eta V}, \tag{27}$$

where *m* is the magnetic moment of the particle, *B* is the magnetic field, κ is the particle shape factor (e.g., for a sphere, $\kappa = 6$), *V* is the particle volume, and η is the dynamic viscosity. This type of asynchrony also appears in the flashing of fireflies and in Josephson junction voltage dynamics [69].

As can be seen from Equation 27, one of the physical properties that the nonlinear rotation rate depends on is fluidic drag. When a bacterium (or bacteria) attaches to a rotating magnetic particle, the particle's volume and shape are drastically changed. This

produces more drag and, therefore, the nonlinear rotation rate slows down considerably. This technique can determine a change in drag caused by the attachment of a 1.0 μm particle to a 1.9 μm nonlinear rotating magnetic microsphere [22]. Even the binding of a single bacterium is straightforward to detect by attachment to a 2.0 μm sphere; in fact, the nonlinear rotation rate was observed to slow down by a factor of ~3.8 on average, which corresponds to 280% increase in rotation period [5]. The technique is also dynamic in the sense that a change in drag causes a direct change in the nonlinear rotation rate; so the growth of an attached bacterium would cause further changes in drag. It is in this way, through changes in drag, the bacterial growth can be monitored, potentially enabling rapid antimicrobial susceptibility measurements.

The ability to detect and monitor biological agents is of fundamental importance for rapid and accurate medical diagnostics. Recent investigations have focused on the development of micro- and nanoscale oscillating systems as novel detection schemes that are both ultra-sensitive and rapid. Detection methods utilizing oscillatory systems offer a powerful and diverse group of extremely sensitive tools that have demonstrated single biological agent detection [5,70,71,55,72,73]. Micro- and nanoscale oscillators can be classified into several general categories, some of which include resonant nanomechanical (NEM) cantilevers [55,72], rotational-based oscillators bound to a substrate via carbon nanotubes [74], and fluid-based magnetically actuated systems [45]. A key distinction of the latter systems is that they exhibit a nonlinear behavior that enables a new sensing scheme, a scheme where viscous effects can be used to great advantage [5] – unlike the application of cantilevers [75-77,73], which work best in air or vacuum surroundings.

We note here that drag depends on volume rather than mass. This makes detection in viscous media both possible and desirable, and therefore facilitates continuous monitoring for bacterial growth applications. Indeed, nonlinear micro-oscillators have the property that both single bacterium detection and its growth can be performed with the same technique, thus allowing for combined rapid detection and growth monitoring – Figure 20.

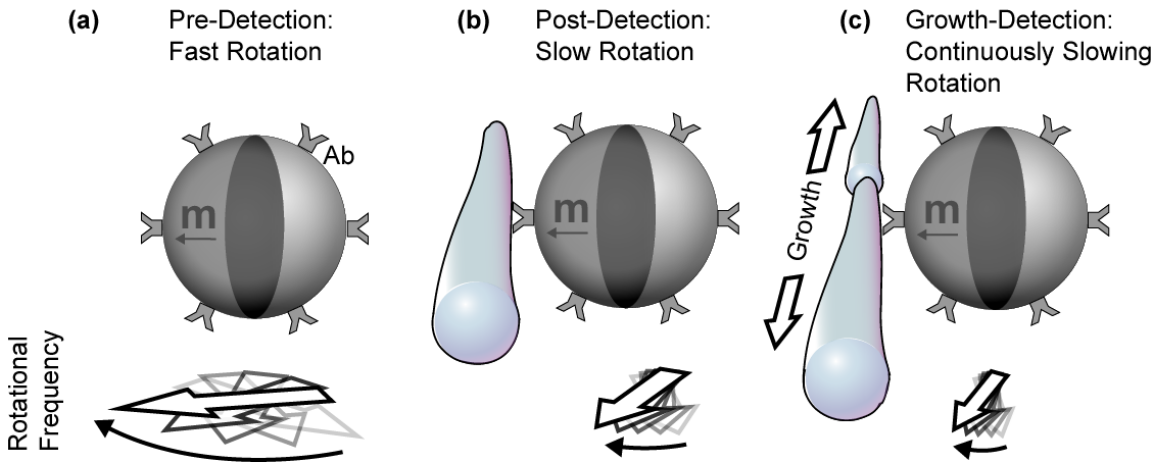

Figure 20: Schematic of the nonlinear rotation rate of a magnetic microsphere functionalized with an antibody (a) with no attached bacteria, (b) with one bacterium, and (c) after bacterial growth. The rotation rate slows as more bacteria are attached or grow on the surface of the particle.

Despite limiting factors, cantilevers have been used for the detection of single biological agents, such as bacteria; however they operate dynamically with high sensitivities only in air or vacuum environments [55,72]. Indeed, cantilevers are capable of detecting pathogens in fluids, but not when operated in a dynamic mode. Instead, they utilize static deflection, which allows for detection in fluids [78], but not for continuous monitoring of the growth dynamics of attached pathogens. Cantilevers have been used to monitor bacterial growth, but the cantilever was not operated in a fluid, rather in a "humid

environment" [79]. Most recently, Burg et al. [73] have demonstrated that single bacterial cells in fluid can be detected, when the fluid is flowed through the *interior* of a cantilever.

There remains a clear need for small scale oscillating systems to be operable in fluids, specifically so that the fluid environment can be continuously monitored. This feature is what makes nonlinear magnetic oscillators both significant and unique. Namely, they can be used to detect a single bacterium and have a sensitivity that will allow for monitoring subsequent bacterial growth [5,22], which in turn, will allow for rapid antibiotic susceptibility measurements. Therefore, in this paper we present a new method that utilizes a laser diode and a photodiode detector device for measuring the linear-to-nonlinear rotational dynamics of magnetic microspheres.

Experimental

The prototype housing was printed with acrylonitrile butadiene styrene (ABS) plastic, using a rapid prototyping machine (Dimension FDM Elite rapid). The housing was fabricated to interface with standard Thorlabs parts, including an unamplified photodiode and a 4.5 mW 635 nm focused laser – see Figure 21. The laser was mounted on a small translation stage that allowed for alignment in the sample plane. The laser was focused through the sample plane, where a single particle was held in an inverted droplet. This forced the particle to the center of the droplet, where the particle remained as it was rotated by an external magnetic field. The rotating magnetic field was produced using either a set of perpendicular coils or a cylindrical magnet (magnetized along the diameter) attached to a stepper motor. While the rotating magnet setup accomplishes asynchro-

nous rotation, it is not as precise as a set of coils, due to the asymmetry of the field produced by the magnet.

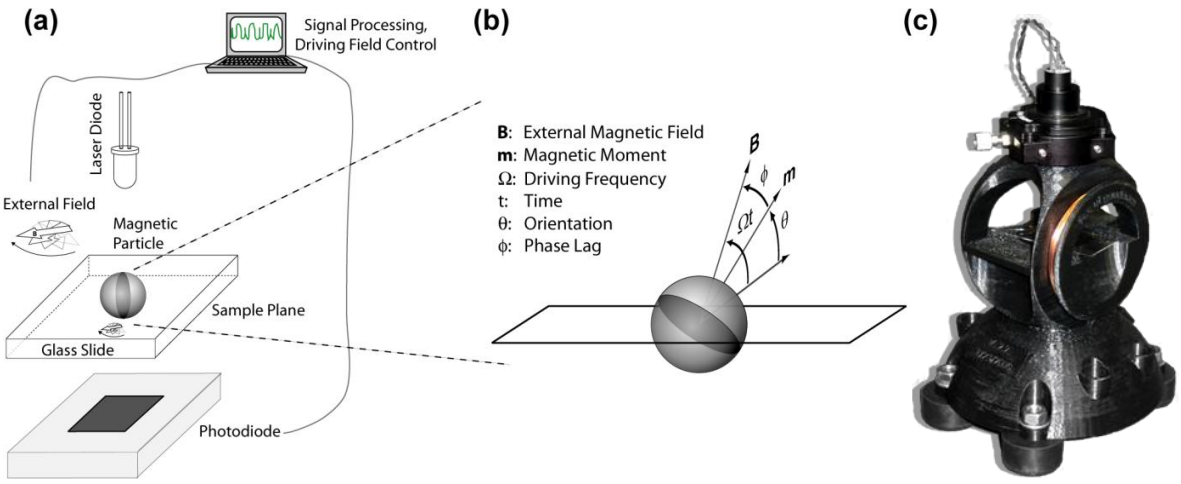

Figure 21: Schematic illustration showing the (a) experimental setup used for the prototype and (b) relevant parameters for particle rotation. (c) Image of constructed prototype, which has dimensions of 14 cm x 10 cm x 10 cm.

Magnetic particles with an approximate diameter of 40 microns and with a streptavidin coating were diluted to approximately 1 particle/ 10 μL (Spherotech, Inc.) in phosphate buffered saline (PBS). For preliminary experiments with bacteria, particles were coated with biotic conjugated anti-*E. coli* antibodies and diluted in Luria Broth growth media. A single 10 μL droplet of the diluted solution was placed onto a coverslip and inverted on the sample plane of the prototype. The laser was then focused through the particle in the droplet. The method also works when more than one particle is in the droplet, but for maximum sensitivity to drag and viscosity, a single particle was isolated. A low power bright field microscope was used to examine the droplet and confirm that a single particle was in the droplet.

The photodiode on the prototype device was interfaced to a computer via a USB data acquisition (DAQ) board UE9 (Labjack, Inc.). The data were then acquired, saved, and analyzed using a program written in LabVIEW 8.5 (National Instruments). The program takes the periodic data of the forward scattered light and measures the period (or frequency) of the rotation data, using an autocorrelation algorithm. The data are then taken for various external driving frequencies.

Results and Discussion

The raw voltage-time characteristics of the photodiode were obtained and analyzed in real-time – see Figure 22 parts a and b. When a particle is in the beam of the focused laser, the laser light is scattered. The photodiode is positioned on the prototype device so that the varying intensity of the forward scattered light can be measured. As the particle rotates in the beam, the light is scattered differently for varying orientations. Therefore, the photodiode measures the particle orientation through variation in the forward scattered light. The magnetic microsphere has enough inherent optical asymmetry to create these varying intensities. Figure 22a shows the raw photodiode data for a single 40 μm magnetic microsphere rotating synchronously with the external field (both the particle and the field are rotating at 0.23 Hz). Figure 22b shows the raw data for the same particle, but at a higher driving frequency of 0.6 Hz. At this driving frequency the particle is asynchronous with the external field and therefore, has a lower average rotation frequency of 0.06 Hz.

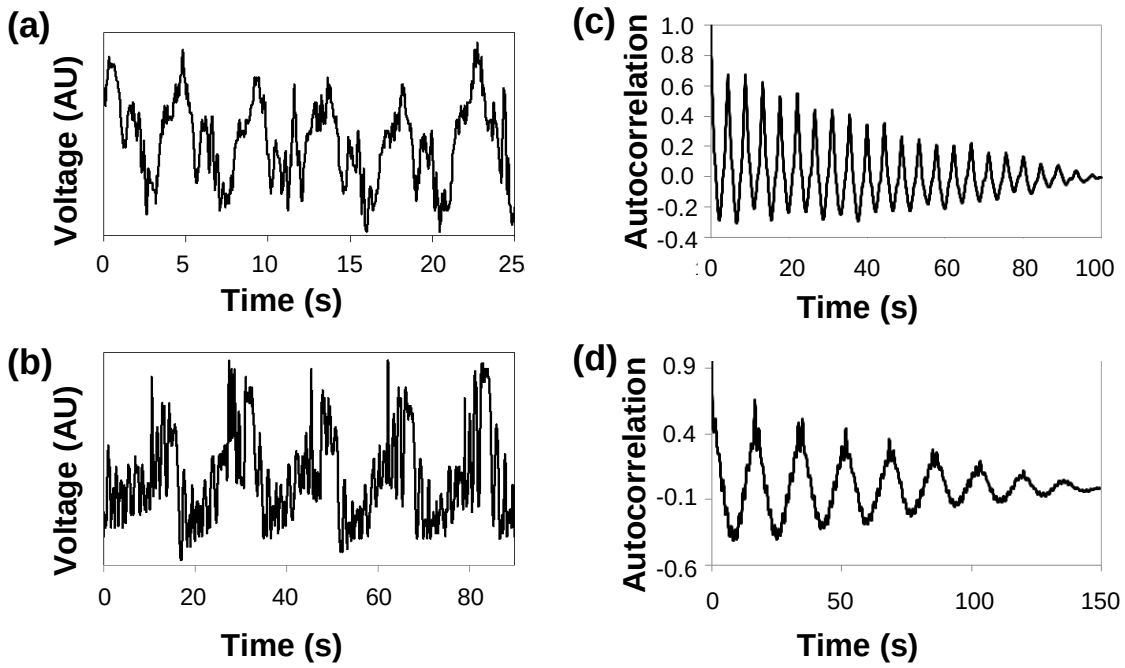

Figure 22: Prototype data from the photodiode, where the magnetic microsphere is rotating in (a) the linear regime (synchronous) at a driving rate of 0.23 Hz and (b) in the nonlinear regime (asynchronous) at a driving rate of 0.6 Hz. Autocorrelation of photodiode data for (c) synchronous data, where the particle rotation rate is 0.228 Hz and (d) raw asynchronous data, where the particle rotation rate is 0.058 Hz.

An autocorrelation algorithm was implemented to determine the rotational period of the raw data streaming to the computer, thus allowing the real-time monitoring of the properties of the particle (e.g. magnetic moment, volume, shape) or the particle's environment (e.g. viscosity). We have performed preliminary experiments where the growth of attached *E. coli* was rapidly monitored and where viscosity changes, resulting from a one degree Celsius change in surrounding water, were measured. We were also able to monitor the rotational dynamics of a single 20 μm magnetic microsphere, using the same configuration. With further optimization of the laser focus, smaller particles can be monitored using this laser and photodiode setup.

Indeed, measuring the rotational rate of a single magnetic microsphere is straightforward using this method. A full characterization of the linear to nonlinear rotational dynamics allows for a more accurate determination of the physical parameters of the system. This was accomplished by interfacing a stepper motor, with an attached magnet, to a computer. The external driving frequency was incremented, and at each step, a value for the rotational rate of the particle was measured. This allowed for an entire linear-to-nonlinear curve to be obtained – see Figure 23. The data are in good agreement with equation (26), but exhibit some variation from the fit. This variation from Equation (26) is a result of nonuniformities in the rotating magnetic field [59]. These nonuniformities can be corrected by implementing electromagnets to create a rotating field, rather than a permanent magnet.

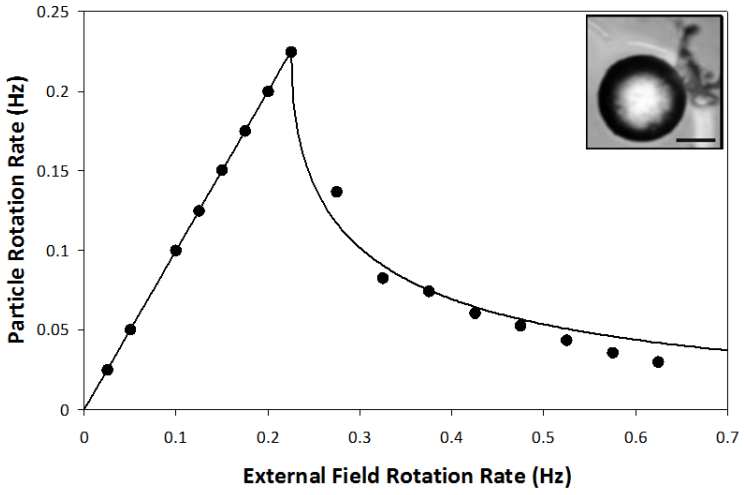

Figure 23: The average rotational rate of a 40 μm single magnetic microsphere as a function of the external field rotation rate, where the circles are experimental data points and the line is a least squares fit from Eq. 1. Inset: Bright field microscopy image of the particle, where the scale bar is 20 μm.

Conclusion

To the best of the authors' knowledge this is the first measurement of asynchronous rotation without a microscope or a CCD camera. While experimenters to date have had much success using microscopy techniques, there is still a need for a simpler and more robust stand-alone instrument, especially for potential usage in clinical diagnostics. This new method of monitoring the nonlinear rotational dynamics of magnetic microspheres has potential for many biomedical applications.

CHAPTER V:

Self-assembled magnetorotation sensors for bacterial drug resistance

Bacterial antibiotic resistance is one of the top concerns of modern healthcare worldwide [80]. The development of rapid growth based diagnostics is a key in addressing this problem [1,2]; faster diagnostic tests will reduce inappropriate antibiotic use [81], decrease health care costs [82], reduce the prevalence of antimicrobial resistance [82,83], and lower mortality rates. Here we introduce self-assembled magnetorotation sensors for antibiotic susceptibility testing (AST), specifically in measuring the minimum inhibitory concentration (MIC) value, and demonstrate a prototype that can monitor multiple sensors simultaneously. We rapidly measured the MIC for uropathogenic *Escherichia coli* isolate using the self-assembled magnetorotation sensors. Reducing the time required to determine the MIC value has an important clinical impact, as patients may be administered more appropriate and adequate antibiotic therapies earlier, which subsequently may lead to more effective treatment [84,81,82].

Introduction

The rotational rate of magnetic particles within a rotating magnetic field is proportional to the drag experienced by the particles when they are driven in the so-called

asynchronous regime, which enables their use as biosensors [4-6,8,9,18,22,24,59]. These asynchronous magnetic bead rotation (AMBR) biosensors have been used to detect and monitor the growth of bacteria at the single cell level [5,6]. However, observing the rotation of spherical microscopic objects usually requires the use of a microscope. Here we introduce self-assembled magnetorotation sensors that are based on the AMBR technology and also demonstrate a prototype that can be used to monitor multiple sensors simultaneously without the use of a microscope.

In an external magnetic field, a magnetic dipole moment is induced in each superparamagnetic microparticle and the particles self-assemble to various structures, including rods and disk-like clusters [85-89]. Previous applications of these self-assembled magnetic microparticle clusters include micropumps in microfluidic channels [90,91].

In a rotating magnetic field, these clusters exhibit asynchronous rotation similar to single particles, and can, therefore, be used for sensing applications. We show that when the shape of the assembled magnetic particle clusters remains unchanged in time, their rotation rate can be used to monitor changes in drag. These self-assembled magnetorotation sensors are used to measure the MICs of uropathogenic *E. coli* bacteria. A standalone prototype for monitoring 16 self-assembled AMBR sensors simultaneously is constructed and it is used to observe bacterial growth within 90 minutes.

Disklike clusters of magnetic particles can be formed in water or PBS-buffer, but these clusters continuously change their shape in rotating magnetic field, a similar behavior reported by Nagaoka et al. [85,92]. Modifying the surrounding media by adding casein stabilizes the clusters within a magnetic field, i.e. do not change shape in time. The

same behavior was observed with particles decorated with specific antibodies. Mueller Hinton (MH) Broth, the general growth media used for culturing bacteria for AST in clinical laboratories, contains casein (which is also how its use in self-assembled AMBR sensors came about serendipitously, enabling rigid instead of ever-changing cluster structures to be formed).

As shown previously, a superparamagnetic particle placed in a rotating magnetic field (at sufficiently high frequency) experiences a constant torque in the direction of the rotating field [6,37]. It is, therefore, a reasonable approximation that our roughly circular discs also experience a torque that is constant in time. This approximation is certainly valid when one is interested in time steps larger than the rotational period of the driving field. Given this assumption, the rotational period of an object under constant torque in fluid is only a function of its fluidic drag (if surface interactions can be neglected). Therefore any changes in the drag of the cluster can be observed by measuring its rotational period in time. The changes in drag are due to change in the size of the cluster, either from spreading between particles or bacterial growth on edges, or change in viscosity of the medium; see Figure 24b.

Results and Discussion

The experiments were performed in a hanging droplet sample, where the self-assembled AMBR sensor was formed on the air-water interface of an inverted 2 µl growth media droplet. The reason for using an inverted droplet sample was three-fold: i) to eliminate surface interactions ii) to use gravity to form the clusters in a reproducible

location at the bottom of the droplet, therefore "self-aligning" iii) to use the inverted droplet as a lens for magnification purposes (Figure 24a), which is useful for off-the-microscope measurements, and forms the basis of the 16 well prototype device introduced below.

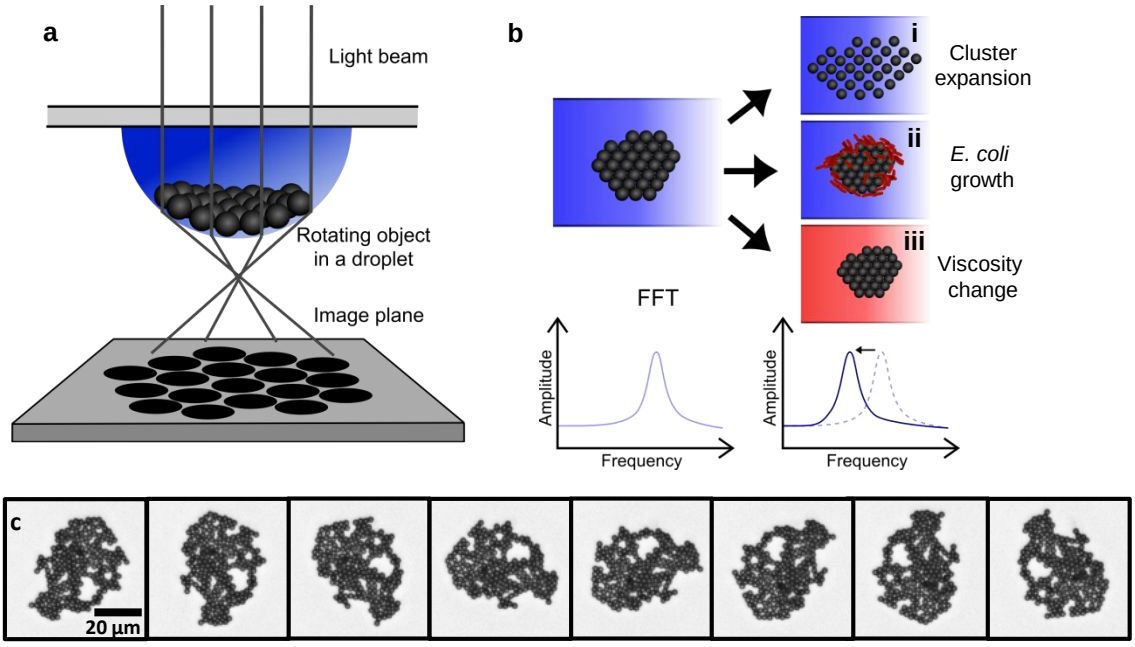

Figure 24: a) A schematic illustration of the droplet lensing effect used to amplify the rotational signal: an LED or laser light is focused by the droplet curvature, magnifying the 'image' of the particle cluster by 100-fold. After the magnification, the rotational period can be observed using a photodetector, which observes a periodic signal corresponding to the rotational period of the cluster. b) The rotational period of the cluster changes accordingly when i) the cluster expands, ii) bacteria etc. attach to the cluster, or iii) the viscosity of the surrounding fluid is changed. The rotational period of the cluster can be measured using the Fast Fourier Transform (FFT), and observing the peak location. c) An optical microscopy image sequence of a self-assembled magnetic particle cluster rotating asynchronously in a rotating magnetic field. Images are taken every 400 ms, magnetic field frequency is 20 Hz with 1 mT field strength. The resulting rotational period of the cluster is 1.7 s.

Using an optical microscope to simultaneously measure the rotation rate of the clusters and monitor bacterial growth, we measured the MICs of two antibiotics for uropathogenic *E. coli* (see Figure 25a-c).

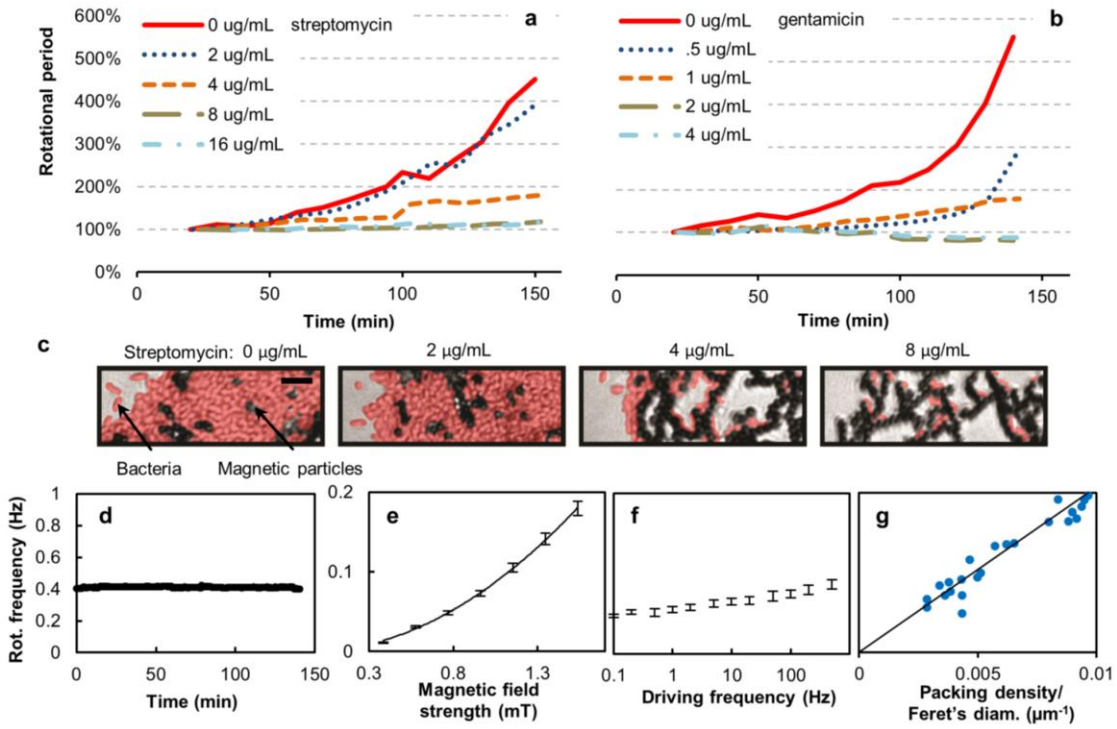

Figure 25: a-b) The rotational signal frequency of magnetic particle clusters used to observe the growth of uropathogenic E. coli with different amounts of antibiotics (streptomycin and gentamicin). When the antibiotic is ineffective the bacteria keep growing and slow down the rotation of the cluster, and when it is effective the growth is inhibited keeping the rotational period constant. The data points are taken every 10 minutes and connected for clarity. c) False colored optical microscopy images of the cluster sensors in different concentrations of streptomycin (data in part a) at time 160 minutes, showing a part of the cluster to highlight the presence or absence of the bacteria. Bacteria are colored red, and magnetic particles are black. Scale bar is 10 µm. d) The rotational frequency of a typical self-assembled AMBR sensor as a function of time, where a few obvious outliers have been removed. The standard deviation of the frequency is 0.7 %. e) The rotational frequency of a magnetic particle cluster as a function of the magnetic field strength. The data is fitted to squared relationship. f) The rotational frequency as a function of the driving frequency on a semi logarithmic axis. The error bars are the deviation between four similar sized clusters (roughly 800 particles per cluster. g) The rotational frequency of many clusters as a function of the packing density divided by the Feret's diameter (maximum caliber) of the cluster. There is a good correlation.

The self-assembled AMBR sensors enabled rapid MIC measurements and the determined values agreed with values obtained with the traditional microdilution method.

The clinical MIC of the uropathogenic *E. coli* isolate was 16 µg/mL for streptomycin and 2 µg/mL for gentamicin, determined with an FDA approved automated system for susceptibility tests, Vitek 2. Using the self-assembled AMBR sensor, the MIC values that we measured were 8 and 2 µg/mL (see Figure 25a-b), which are consistent within one doubling dilution of the reference MIC [93].

To characterize our self-assembled AMBR sensors, we measured the rotation rates of multiple clusters as a function of time, magnetic field strength, frequency, and cluster size (Figure 25d-g). The rotational period (reciprocal of the rotational frequency in Hz) of an unperturbed AMBR cluster is stable, showing only 0.7 % variation in time (Figure 25d). The rotational frequency of the AMBR cluster has a quadratic dependence on the driving magnetic field amplitude (at 100 Hz), which is expected from the literature [6,37], as is the weak dependency on the driving frequency (Figure 25e and f). Although no correlation was found between the size of the group (area-wise, data not shown), the rotational frequency of the clusters increases with increased packing density of the cluster and decreased Feret's diameter (also called the maximum caliber), see Figure 25g.

A prototype was built by an engineering company (Insight Product Development LLC, Chicago, IL) for the purpose of performing AST testing with the self-assembled magnetorotation sensors (See Figure 26). The design of the prototype was enabled by the self-assembled AMBR sensors and self-aligning and lensing properties of the hanging droplet samples.

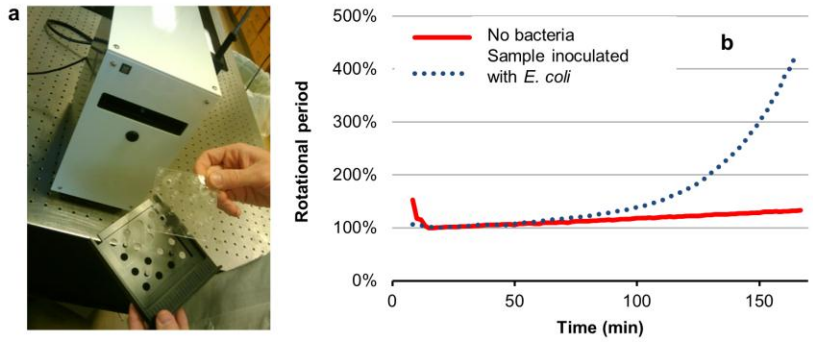

Figure 26: a) An image of the prototype device for rapid AST testing of bacteria using self-assembled magnetorotation sensors. The prototype accepts cards with 16 wells, which can be loaded with different amounts of samples containing a self-assembled magnetorotation sensor with antibiotics and bacteria. The prototype is controlled with a custom computer program written in NI LabView. b) Data from the prototype showing the difference between a sample inoculated with *E. coli* bacteria compared with a sample with no bacteria. The rotational periods are normalized to 1 after initial warming of the sample.

The prototype was designed to work with off-the-shelf electronic components; the rotating magnetic field is generated by passing sinusoidal currents (at 100 Hz) through inductors and the rotation rate of the AMBR sensors is observed by aligning a laser through each of the 16 sample holding droplets (see Figure 24a) and monitoring the laser intensity with photodetectors. The sample holder card holds 16 hanging droplets and is made out of polydimethylsiloxane (PDMS). Data acquired with the prototype is shown in Figure 26b, showing the rotational signal of self-assembled magnetorotation sensors inoculated with bacteria, compared to the sensors with no bacteria present. A difference can be seen within two hours from the inoculation. One of the problems with this generation prototype is the slow evaporation of the droplets through the gas-permeable PDMS card, manifestation of which can be seen in Figure 26b as the slight slowing down of the control rotation.

Methods

Magnetic particles functionalization

Streptavidin functionalized 2.8 μm diameter superparamagnetic particles (Invitrogen, Dynal M-280) were functionalized with biotinylated anti *E. coli* antibodies (Abcam, ab20640-1) using a modified version of the Bangslabs adsorption protocol [94]. Specifically, 100 μl of the M-280 bead stock solution (6-7 × 10^8 beads/mL) was combined with an equal volume of Phosphate Buffered Saline (PBS) with 0.1% Bovine Serum Albumin (BSA) and 0.1% Tween-20 solution, referred to as PBS-TB. Beads were magnetically separated and resuspended in 200 μL of PBS-TB solution. This solution was pipetted into 30 μL of stock antibody solution (4 mg/ml) and mixture was rotated in a 1.5 μl vial at room temperature for 24 hours, end-over-end at 60 rpm, and then allowed to sit at room temperature for 1.5 hours. Particles were magnetically separated and washed three times in PBS and resuspended in 1 ml of PBS resulting in 6-7 × 10^7 beads/ml concentration.

Bacterial growth conditions

Uropathogenic *Escherichia coli* isolate (Clinical Microbiology Laboratory, University of Michigan Hospital) was grown on Mueller Hinton (MH) agar media in 37 °C for 18-20 hours, suspended in Mueller-Hinton broth and diluted to 0.5 McFarland standard, which corresponds roughly to 1.5 × 10^8 CFU/ml.

Binding protocol

To bind magnetic particles to the bacteria, 12.5 µl of the bacteria solution was combined with 10 µl of anti-*E. coli* coated magnetic beads and an additional 77.5 µl MH broth. The vial containing this mixture was shaken in dish on a rocking platform shaker at ~180 rpm at 37 °C for 1.5 - 2 hours, to bind the bacteria to the magnetic beads. Bacteria coated beads were then removed from solution using a handheld magnetic separator (Bio-Nobile, PickPen 1-M), temporally released into 300 µl of MH, removed from that solution, dipped but not released in a second vial of MH and finally resuspended in 250 µl of MH, resulting in a $3 \pm 0.5 \times 10^6$ beads/ml.

Samples of bacteria coated beads were then combined with equal volumes of MH containing varying concentrations of antibiotics. Two 1.55 µL droplets of each antibiotic concentration were deposited onto 1.5 mm PTFE coated slides (Tekdon inc., 244-041-120) and inverted to create inverted droplets. Sample was taped and sealed using a greased (Apiezon, L grease) custom-cut 1.6 mm thick rubber spacer and a glass slide.

Beads were pulled to the bottom of each droplet by holding the sample above a permanent magnet for 20 seconds. Sample was then placed within pair of Helmholtz coils on Olympus IX71 inverted microscope, in a custom built on-stage incubator that was held at 37 ± 1.5 °C. One of the two sets of coils was turned on creating a lateral 100 Hz oscillating 1 mT magnetic field to align particles. After 30 seconds of 1D field, the second set of coils was turned on, creating an equivalent, orthogonal oscillating field 90° out of

phase, resulting in 100 Hz 1 mT rotating magnetic field in the imaging plane. This rotating field formed and rotated clusters of beads at the bottom of the hanging droplets.

One droplet of each concentration was selected to observe. The only selection criterion was that the cluster not be visibly contaminated with foreign particles. Videos of each cluster were taken at ten-minute intervals at 50 fps using a digital camera (Basler, piA640-210gm) with 20x objective. Rotation rate was determined using a LabView program called StaT tracker (by the University of St Andrews Optical Trapping Group), which was modified to observe angular changes.

Conclusions

We report on the development of a self-assembled AMBR sensor, and its use for antimicrobial susceptibility testing (AST). The minimum inhibitory concentration (MIC) of uropathogenic *E. coli* to streptomycin and gentamicin was measured using the method. A new method for the visualization of the AMBR biosensor signal is presented, and based on it a stand-alone prototype for monitoring 16 self-assembled AMBR sensors simultaneously is constructed and used to observe bacterial growth within two hours.

CHAPTER VI:

Conclusions and future work

In the previous chapters we have explored the various applications and developments of the emerging AMBR (asynchronous magnetic bead rotation) sensors. Due to the broad applicability of the sensor platform, the most appealing potential applications are still taking shape. This dissertation summarizes the development work we have done with AMBR sensors in the past three year. The first chapter gives the historical context and the basic introduction to the work that I, and other people in the Kopelman laboratory have done. Chapter II – V summarize original research which is either published in peer reviewed journals or is going to be submitted. In the second chapter we investigated the effect of the bead frequency on the sensor sensitivity, and demonstrated 145 Hz critical frequency of an AMBR sensor, resulting in a 59 nm theoretical sensitivity in the bead radius. In the third chapter the extreme volumetric sensitivity of the AMBR biosensor is used to measure the growth of individual bacteria, with up to 80 nm sensitivity to the cell length. In the fourth chapter we introduce a compact sensor for the observation of AMBR biosensor signal, since the work done in Chapters II and III was done using an optical microscope. We demonstrate a novel method for observing AMBR biosensor signal using a combination of a focused laser and a photodiode, which marks the first AMBR observa-

tion without an optical microscope. In the search for more robust AMBR biosensor for antimicrobial susceptibility testing, Chapter V introduces self-assembled AMBR sensors. Based on the self-assembled AMBR sensors we design a robust 16 well prototype, and validate it toward antimicrobial susceptibility testing. The minimum inhibitory concentration of a uropathogenic *E. coli* was measured in two hours. In summary the work presented here transformed a biosensor which had to be observed with a powerful microcope, into an extremely robust and reproducible inexpensive off-the-microscope biosensor with the possibility for massively parallel measurements of up to thousand biosensors (see the section below). There is a great need for such biosensors in research including drug discovery, and in the clinical setting for the rapid observation of bacterial growth.

To increase the throughput and simplify the sample preparation, it is possible to integrate AMBR biosensors with microfluidics [24]. By combining the small size and ease of sample preparation made possible by microfluidics technology and the high sensitivity of AMBR sensors, we imagine that it will be possible to achieve a biosensor that is especially suitable for point-of-care settings.

The sections below introduce some aspects of the AMBR biosensor that will be further developed in the future. The sections include: the use of a CMOS pixel array for the parallel measurements of AMBR biosensor; a novel pre-enrichment separation step that can be used to separate magnetic beads by their volume; and lastly a method for fabricating neutrally buoyant magnetic beads for AMBR biosensors.

CMOS pixel array for massively parallel AMBR measurements

Methods for observing multiple AMBR biosensors in parallel are needed for even wider applicability of the platform. One potential approach, introduced below, is to use the pixel array found in digital cameras, where the pixels are 2 – 10 μm in diameter. The theoretical limit of the number of parallel measurements is thousand sensors per single standard size CMOS array, which can be found even in most inexpensive cameras. The sample can be placed directly on top of the pixel array (protected by a thin glass layer), and if it is illuminated by a collimated light beam directly from above, the AMBR sensor draws a "shadow image" on the pixel array (Figure 27 a), and the rotation can be observed from the modulation in the shadow image, provided that the sensor is not perfectly spherical. As a preliminary result we therefore used a CMOS camera pixel array (with no lenses) and an LED light source to measure the rotation of an elongated 16 μm particle, Figure 27. We expect that any AMBR sensors with larger than 15 μm diameter can be measured using the same principle, including yeast cells and the cluster AMBR sensors introduced in Chapter V. Furthermore, a single CMOS array is large enough to measure the rotation rates of up to a thousand of such sensors simultaneously, which can be done using particle tracking and frequency analysis software. Due to the nature of the collimated light, no focusing is needed, making the parallel observation of sensors feasible while using off-the-shelf electronic components, such as a CMOS camera and an LED light source.

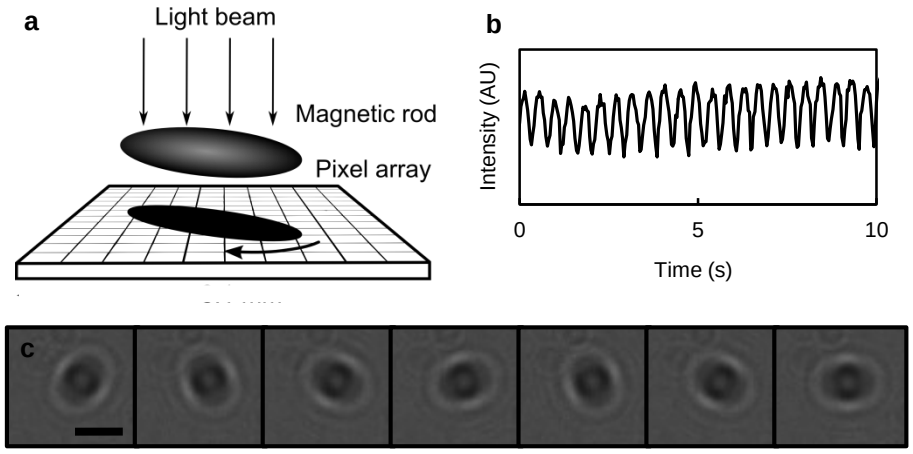

Figure 27: The rotation of a single 16 µm particle rotation observed using a CMOS pixel array. a) A schematic of the principle how to use a CMOS camera pixel array without lenses to observe particle rotation. b) The light intensity of a region of interest, modulated by the rotation of the particle. The modulation can be used to measure the rotation rate of the particle. c) Images of an elongated 16 µm particle taken with a CMOS pixel array, rotating asynchronously in a rotating magnetic field. The sample was placed on top of the pixel array, separated by a thin glass slide. The time between frames is 150 ms, and the length of the scale bar is 15 µm. For experimental methods, see Appendix C.

Sorting magnetic particles by their critical AMBR frequency

Magnetic isolation of the target of interest from a patient's fluid sample is an important sample preparation method. Magnetic isolation is also widely used in detecting pathogenic bacteria from food samples in a similar fashion. Since any magnetic particles can be used as AMBR biosensors, the "whole cell separation method" can be used as a preparation step for measuring bacterial growth with the same magnetic particles, as the bacteria will have already been attached, allowing for seamless integration of the two methods. However, during whole cell separation of bacteria, only a subpopulation of the

magnetic particles have cells attached, and in AMBR biosensor growth applications it is crucial that the bacteria-to-beads ratio is sufficiently large, otherwise the signal is lost in the noise. Therefore, a useful pre-step would be to isolate the subpopulation, which has bacteria bound to it, where the bacteria-to-beads ratio is at least one.

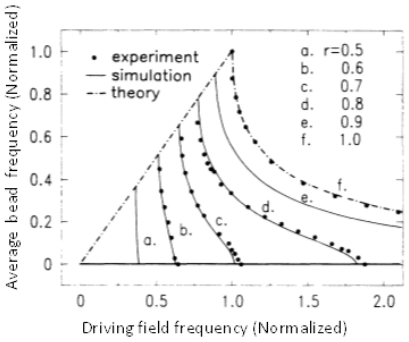

Figure 28: Magnetic particle rotation frequencies with varying field ellipticity. Where r = ratio of 'x component amplitude' vs. 'y component amplitude' of the magnetic field. The more elliptical the field, the lower the critical and stopping frequency (ie. the frequency above which the particle does not rotate).

Magnetic microparticles can be sorted by their critical asynchronous frequency by 'rolling' on a surface. By applying an 'elliptical' rotating magnetic field, only particles that possess a critical frequency above a certain value will rotate. The magnetic particles' rotation frequencies within elliptical rotating magnetic fields with different x and y component strengths can be seen in Figure 28 [59]. The critical frequency is inversely proportional to the volume of the rotating body, and therefore this method can be used to separate, for example, bare magnetic particles from magnetic particles with a single cell attached after binding procedure.

Similar magnetic bead sorting with rotating magnetic fields has been described by Yellen et al. [15]. However it is fundamentally different in that it relies on the migration of the magnetic field gradients and also requires the fabrication of micropatterned magnetic material.

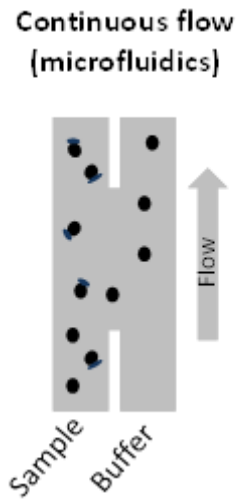

Figure 29: Bare magnetic particles are separated from the ones that have a bacterium bound in a microfluidic channel. Example of the separation by the critical AMBR frequency, where the elliptical field rotates from left to right and out of the image plane. Black spheres are magnetic particles and blue ovals denote bacteria.

Naturally buoyant magnetic particles

High magnetic moment particles are required for many applications; however a high magnetic moment also means a high fraction of magnetic material. Since the specific gravity of most of the used magnetic materials is many times higher than water, the settling of the magnetic particles becomes an issue in some applications. Thus far, we have considered only AMBR sensors that are driven at the bottom of the fluid, at the water-air interface or on the surface of the sample container. However, it could be advantageous for some studies to observe freely floating AMBR sensors, with no interface or surface interactions. Such AMBR biosensors need to be neutrally buoyant (have a characteristic specific gravity of one, or adjusted according the density of the sample fluid). A method to fabricate neutrally buoyant magnetic particles is explained below. Using the same technique, the specific gravity of the particles can be tuned to the desired value.

Non-magnetic particles that have a low specific gravity can be turned magnetic by coating them with magnetic material. This can be easily done with vapor deposition of nickel or cobalt. At the same time the specific gravity of the particles is increased, and by adding the right amount of coating, the density can be tuned.

For example, 10 um diameter hollow glass spheres have a density of 0.8 g/cc, and, therefore, they would be turned neutrally buoyant by coating the particle with a 150 nm layer of Nickel (8.9 g/cc) and 5 nm gold (19.3 g/cc). Considering that 10 um particles with a 300 nm Nickel coating have a 3×10^{-4} Am² magnetic moment and 150 a Hz critical frequency [95] and that the critical frequency is proportional to the nickel coating volume [22], 10 um particles with 150 nm thick Ni coating would be expected to have a magnetic moment and critical frequency at half of those values (1.5×10^{-4} Am² and 75 Hz). See Figure 30 for a schematic.

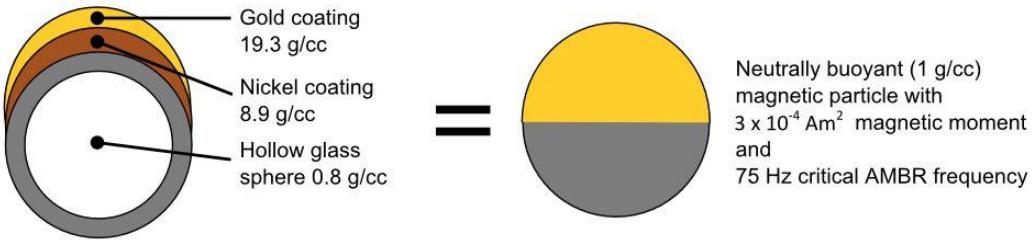

Figure 30: Neutrally buoyant magnetic particle made by half coating a hollow glass sphere. Coating thicknesses are exaggerated for visualization.

APPENDICES

APPENDIX A:

Ferrohydrodynamics and the early history of AMBR

The term ferrohydrodynamics was introduced in 1964 by Neuringer and Rosensweig [96] in "Ferrohydrodynamics" which is considered as the first publication in this field of science. The research on ferrohydrodynamics has grown due to the interest in using ferrofluids in the presence of magnetic fields in order to convert magnetic energy into motion with no moving parts, and the increase of viscosity of magnetorheological (MR) fluids in applied magnetic fields. Ferrofluid dynamics in rotational magnetic fields were first studied experimentally by Moskowitz and Rosensweig in 1967 [25]. The physics behind the rotation were not understood, and it was believed that each particle follows the field with a phase lag. A theoretical study of single ferromagnetic (FM) and superparamagnetic (SPM) particles in rotating magnetic fields was conducted two years later to answer some of the risen questions [26]. Caroli and Pincus found out, correctly, that for FM particles there is a critical frequency below which the particle rotates synchronously with the rotating field, but they got the behavior slightly wrong above the critical frequency: their results state that the particles “oscillate about their initial positions with a characteristic frequency ω_p” :

$$\omega_p = \sqrt{\Omega^2 - \Omega_c^2}\,, \tag{A1}$$

where Ω is the driving frequency and Ω_c is the critical frequency. Instead the correct behavior is the following: "particle rotation rate which is steady but which has superimposed on it an oscillatory component of relatively small magnitude; the mean particle rotation rate decreases as [the driving frequency] increases" as Popplewell, Rosensweig and Johnston deciphered correctly from their numerical integrations of the equations of motion in 1990 [27]. The frequency of the oscillations was indeed correct in Caroli's and Pincus' paper, and the value they acquired for the critical driving frequency was:

$$\Omega_c = \frac{MB}{6\eta} = \frac{mB}{\kappa\eta V_{mag}}\,, \tag{A2}$$

which indeed agrees with the more recent model [4]. Caroli and Pincus also touched on the behavior of single SPM particles, ending up with a critical frequency for a single SPM particle in a rotating magnetic field

$$\Omega_c^{SPM} = \frac{K(\chi B)^2}{6\eta}\,, \tag{A3}$$

where χ is the static susceptibility given by the Langevin formula and $K > 0$ is the anisotropy constant ("valid when the system thermalizes [reaches thermal equilibrium] in a time short compared to all the characteristic times of the problem"). The behavior of the SPM particles above the critical frequency was found to be the same as for ferromagnetic

particles (namely eq. A1 with Ω_c^{SPM} substituted for Ω_c), where they possibly made the same mistake of ignoring the overall average rotation forward. The author was not successful in finding other studies on single SPM particles in rotating magnetic fields. Caroli and Pincus calculated a value for Ω_c^{SPM} at 300 Kelvin, yielding $\Omega_c^{SPM} \sim 10^9\ Hz$. However the Neel relaxation time (and presumably therefore also Ω_c^{SPM}) has an exponential dependence on the particle volume, and therefore a small change in the particle radius changes the critical frequency dramatically.

APPENDIX B:

Measuring the growth of a yeast cell with AMBR biosensor

Asynchronous Magnetic Bead Rotation (AMBR) biosensors have been used previously for detection [5] and growth measurement of single bacteria [6], and in a modified configuration for protein detection [18]. As a platform technology, the AMBR biosensors can be used to measure the growth of any cells (or any volume/viscosity/shape changes), with slight modifications in the sensor. In this implementation, 3 μm magnetic particles were attached to *Saccharomyces cerevisiae* yeast cells (5 – 10 μm diameter), and micropatterned microwells were used to restrict the translation of the sensors and yeast cells. A custom stage top incubator was built to keep the cells at 30 ºC during the experiment (see Figure B1 for the setup schematic). The rotational periods of the sensors were measured using a microscope and video analysis software.

Magnetic particles are bound to the yeast cells using specific antibodies, which essentially introduces a magnetic moment to the yeast cell. Due to the magnetic moment, the cells (with magnetic particles attached), rotate in a rotating magnetic field, with a rotation rate that is a function of the total volume of the cell. Therefore as the yeast cell increases in volume during budding, its rotational period increases, and the rotation period can be used to observe changes in the cell volume (Figure B1 c).

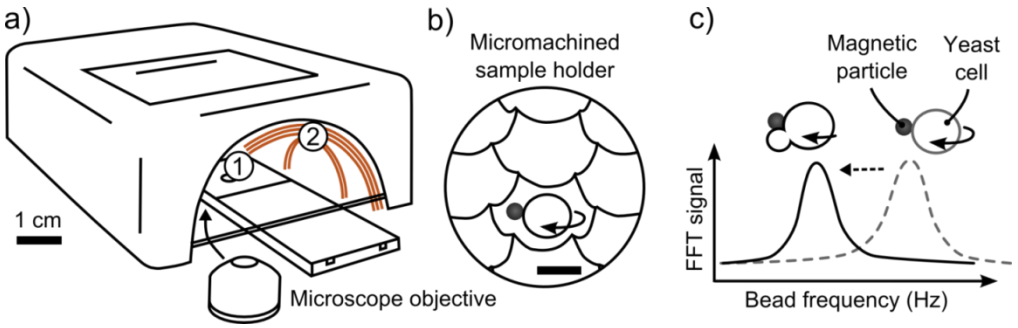

Figure B1. Schematic representation of the AMBR sensors experimental setup. a) On-microscope incubator used for the yeast cell studies, including 1) micromachined sample holder and 2) a set of electromagnet coils for generating a rotating magnetic field. b) Close up of the sample holder where the scale bar is 10 micrometers. c) The change in the AMBR sensor's rotational frequency due to the budding of a yeast cell, symbolized by the small white circle.

Results and Discussion

Two magnetic particles were attached to a single yeast cell and it was separated in a microwell for analysis. We observed a larger than 3-fold increase in the rotational period of the AMBR sensor due to the growth of the single yeast cell over 60 minutes (Figure B2).

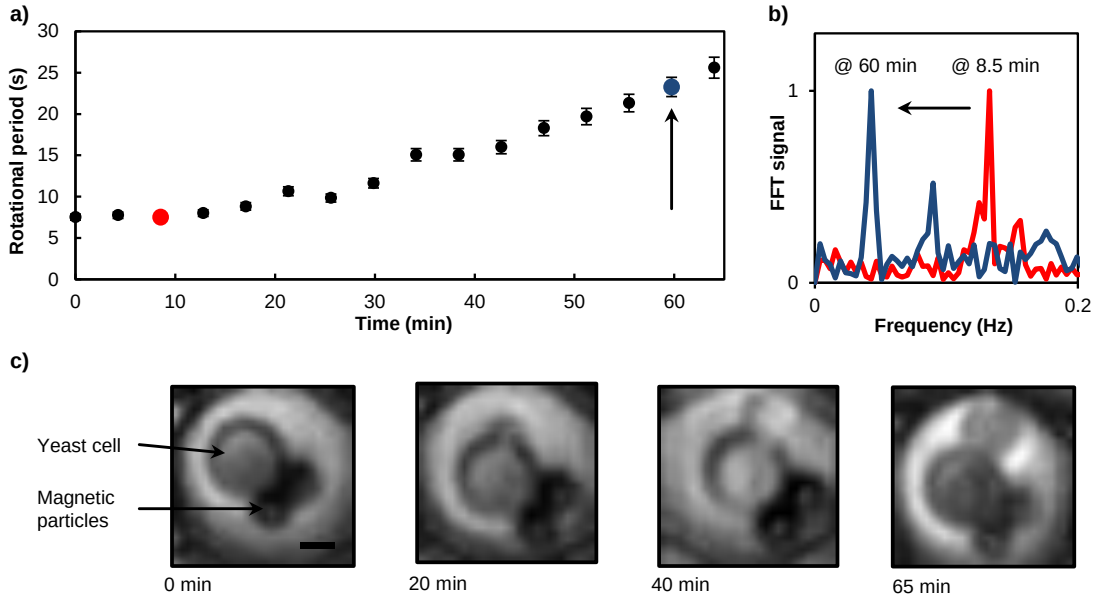

Figure B2. The growth of an individual *S. cerevisiae* yeast cell monitored with an AMBR sensor. a) Rotational period of the AMBR sensor as a result of the budding of the yeast cell in liquid growth media. b) Optical microscopy images of the budding observed in part a). The scale bar is 5 μm. c) The analyzed AMBR sensor signal (Fourier transform) of the data in part a) at 8.5 minutes and 60 minutes.

Asynchronous magnetic bead rotation can be used to transform nanoscale volumetric changes into frequency changes, and the growth of individual yeast cells was measured using that principle as described earlier. However the rotation rate of the sensor was measured using an optical microscope, so the advantage of using the AMBR technique is not great, since the volumetric resolution of the AMBR sensor is only a little better than that of an optical microscope [6]. A low tech method of measuring the rotation of single AMBR sensor particles is needed for a wider applicability of the sensor. One such method has been demonstrated [8], however its scalability is limited due to the need of a focused laser.

Experimental methods

Magnetic particle functionalization

Streptavidin coated 3 μm diameter superparamagnetic particles were further functionalized with *S. cerevisiae* antibodies using the following protocol. A 1 mg aliquot of the magnetic particles (112-05D, Invitrogen) was washed and resuspended in 100 μL of PBS-TB (prepared by adding 0.1% Tween 20 (ACROS Cat. #23336-2500) and 0.1% bovine serum albumin (BSA, Thermo Scientific) to phosphate buffered saline (1x PBS, 1860449 MPBio). The secondary antibodies (25 μL of biotinylated rabbit IgG antibodies, 2 mg/mL ab6720, Abcam) were then introduced and incubated with gentle agitation

(Sarmix MR1, Sarstedt) for 3 hours in room temperature, following with magnetic separation (DynaMag-2, Invitrogen) twice into 100 μL of PBS-TB. The same binding procedure was repeated for the primary antibodies (12.5 μL of rabbit polyclonal antibody to *S. cerevisiae*, 4 mg/mL ab19498, Abcam) and the fully functionalized magnetic particles were then resuspended in 1 mL of PBS-TB and stored in 4 ºC.

Cell culture procedures

The budding yeast *Saccharomyces cerevisiae* cells (ATCC# 2601) were grown on YPD agar (Y100, Teknova) in 30 ºC for 2-3 days prior to experiments. The cells were then suspended in YPD-PB (prepared by adding 0.1% Pluronic F-68 (cat. #2750049 MPBio) and 0.1% BSA to YPD broth (Y5006 Teknova)) in 1-5 × 10^6 yeast cells/mL concentration (obtained by adjusting the turbidity to 0.5 McFarland standard). Magnetic particles were attached to the yeast cells by incubating 25 μL of the previously prepared particle solution with 500 μL of the cell solution with vigorous mixing (1000 rpm) for 60 minutes in room temperature.

Rotation measurements with an optical microscope

After binding, 2-5 μL of the magnetic particle and cell solution was pipetted onto a microfabricated microscope slide with 15 μm wells (cat. #130504, Thermo Scientific) along with 1 mL of YPD-PB solution, and the sample was then ready for growth experiments. The experiments were conducted on two inverted optical microscope setups (Olympus IX71 and IMT-2), with a custom made 30 ºC incubator and two sets of

perpendicular air core electromagnets fitted on top, see Figure B1a. The electromagnets were used to generate a rotating magnetic field, 1 mT in amplitude at 100 Hz frequency. The coils were driven with two sinusoidal signals, 90 degrees out of phase, controlled with a computer program to achieve a uniform rotating magnetic field. To analyze the rotation frequency of the AMBR sensor, continuous videos were acquired at 2-5 fps during the growth experiments. By drawing an area of interest and analyzing the intensity over time by applying a fast Fourier transform, the rotation frequency could be determined, see Figures B2 a and c.

Conclusions

The growth of individual yeast cells was observed using an asynchronous magnetic bead rotation (AMBR) biosensor. During the budding of a yeast cell, a three-fold increase was observed in the AMBR sensor signal.

APPENDIX C:

CMOS pixel array for AMBR measurements:

experimental methods

The rotation measurements were done with a pixel array in Mightex 5 megapixel monochrome CMOS USB camera (BCN-B050-U), which has 2.2 by 2.2 μm pixels. The camera is sold 'board level' with no enclosing, and can therefore be used for these experiments as is. The smaller the distance between the sample and the pixel array, the better resolution can be achieved. That in mind, "windowless" CMOS pixel array that has no glass covering the pixel array would be optimal for this application. Mightex offers such cameras (MCE-B013-UW), however the available models have larger pixel size (5.2 by 5.2 μm), which is not acceptable as it lowers the resolution. As a light source we used a regular low power white LED 20 cm above the sample. We used two pinholes (with roughly 2 mm openings) to minimize stray light; one close to the LED and another one just above the sample. The camera was connected to a PC through a USB port, and the videos were captured using the software that came with the camera. Further image analysis including pixel intensity calculations was done using a free ImageJ program.[67]

A microstep stepper motor driver (G201X, Geckodrive, Inc., Califormia) was used as an inexpensive means to generate amplified sine and cosine signals needed for

rotating magnetic field generation. The G201X accepts 18-80 VDC power supply (1-7A), and requires a step signal that depicts the output frequency (CN0173, Centent co., California). The amplified sin/cosine signals were passed through 2 perpendicular spools of magnet wire (22 AWG, Fisher Scientific), which creates a magnetic field up to 5 mT between the spools, and it can be amplified even further by introducing soft iron cores (WLS44370-35, Sargent-Welch) to the magnet wire spools. Using this setup we were able to generate rotating magnetic fields up to 200 Hz with acceptable quality, in an area of about 1 cm^3, while keeping the cost of the rotating magnetic field setup under $300. The complete setup used to generate the data in A3, including the CMOS pixel array and the LED light source, can therefore be constructed with under $1,000 investment excluding the computer.

BIBLIOGRAPHY

[1] J.H. Jorgensen and M.J. Ferraro, "Antimicrobial susceptibility testing: a review of general principles and contemporary practices," *Clinical Infectious Diseases: An Official Publication of the Infectious Diseases Society of America*, vol. 49, Dec. 2009, pp. 1749-1755.

[2] J.H. Jorgensen and M.J. Ferraro, "Antimicrobial Susceptibility Testing: General Principles and Contemporary Practices," *Clinical Infectious Diseases*, vol. 26, Apr. 1998, pp. 973-980.

[3] D. Schrag, H.S. Garewal, H.J. Burstein, D.J. Samson, D.D. Von Hoff, and M.R. Somerfield, "American Society of Clinical Oncology Technology Assessment: Chemotherapy Sensitivity and Resistance Assays," *Journal of Clinical Oncology*, vol. 22, 2004, pp. 3631 -3638.

[4] B.H. McNaughton, K.A. Kehbein, J.N. Anker, and R. Kopelman, "Sudden breakdown in linear response of a rotationally driven magnetic microparticle and application to physical and chemical microsensing," *Journal of Physical Chemistry B*, vol. 110, 2006, p. 18958.

[5] B.H. McNaughton, R.R. Agayan, R. Clarke, R.G. Smith, and R. Kopelman, "Single bacterial cell detection with nonlinear rotational frequency shifts of driven magnetic microspheres," *Applied Physics Letters*, vol. 91, 2007, p. 224105.

[6] P. Kinnunen, I. Sinn, B.H. McNaughton, D.W. Newton, M.A. Burns, and R. Kopelman, "Monitoring the growth of individual bacteria using asynchronous magnetic bead rotation sensors," *Biosensors and Bioelectronics*, vol. 26, Jan. 2011, pp. 2751-2755.

[7] R. Elbez, B.H. McNaughton, L. Patel, J.K. Pienta, and R. Kopelman, "Nanoparticle induced Cell Magneto-Rotation: Monitoring Morphology, Stress and Drug Sensitivity of a Suspended Single Cancer Cell," *PLoS ONE*, In Press. 2011.

[8] B.H. McNaughton, P. Kinnunen, R.G. Smith, S.N. Pei, R. Torres-Isea, R. Kopelman, and R. Clarke, "Compact sensor for measuring nonlinear rotational dynamics of driven magnetic microspheres with biomedical applications," *Journal of Magnetism and Magnetic Materials*, vol. 321, May. 2009, pp. 1648-1652.

[9] P. Kinnunen, I. Sinn, B.H. McNaughton, and R. Kopelman, "High frequency asynchronous magnetic bead rotation for improved biosensors," *Applied Physics Letters*, vol. 97, 2010, p. 223701.

[10] T. Honda, K.I. Arai, K. Ishiyama, and others, "Micro swimming mechanisms propelled by external magnetic fields," *IEEE Transactions on Magnetics*, vol. 32, 1996, pp. 5085–5087.

[11] B.H. McNaughton, J.N. Anker, and R. Kopelman, "Magnetic microdrill as a modulated fluorescent pH sensor," *Journal of Magnetism and Magnetic Materials*, vol. 293, May. 2005, pp. 696-701.

[12] S.L. Biswal and A.P. Gast, "Micromixing with linked chains of paramagnetic particles.," *Analytical chemistry*, vol. 76, 2004, p. 6448.

[13] L. Zhang, J.J. Abbott, L. Dong, B.E. Kratochvil, D. Bell, and B.J. Nelson, "Artificial bacterial flagella: Fabrication and magnetic control," *Applied Physics Letters*, vol. 94, 2009, p. 064107.

[14] A. Ghosh and P. Fischer, "Controlled propulsion of artificial magnetic nanostructured propellers," *Nano letters*, vol. 9, 2009, pp. 2243–2245.

[15] B.B. Yellen, R.M. Erb, H.S. Son, R. Hewlin, H. Shang, and G.U. Lee, "Traveling wave magnetophoresis for high resolution chip based separations," *Lab on a Chip*, vol. 7, 2007, pp. 1681–1688.

[16] J.N. Anker, C. Behrend, and R. Kopelman, "Aspherical magnetically modulated optical nanoprobes (MagMOONs)," *Journal of Applied Physics*, vol. 93, 2003, p. 6698.

[17] S.Y. Park, H. Handa, and A. Sandhu, "Magneto-Optical Biosensing Platform Based on Light Scattering from Self-Assembled Chains of Functionalized Rotating Magnetic Beads," *Nano Letters*, vol. 10, Feb. 2010, pp. 446-451.

[18] A. Hecht, P. Kinnunen, B.H. McNaughton, and R. Kopelman, "Label-acquired magnetorotation for biosensing: An asynchronous rotation assay," *Journal of Magnetism and Magnetic Materials*, vol. 323, Feb. 2011, pp. 272-278.

[19] H.E. Gaub and H.M. McConnell, "Shear viscosity of monolayers at the air-water interface," *The Journal of Physical Chemistry*, vol. 90, Dec. 1986, pp. 6830-6832.

[20] B.H. McNaughton, P. Kinnunen, R.G. Smith, S.N. Pei, R. Torres-Isea, R. Kopelman, and R. Clarke, "Compact sensor for measuring nonlinear rotational dynamics of driven magnetic microspheres with biomedical applications," *Journal of Magnetism and Magnetic Materials*, vol. 321, 2009, pp. 1648-1652.

[21] J.N. Anker, C.J. Behrend, H. Huang, and R. Kopelman, "Magnetically-modulated optical nanoprobes (MagMOONs) and systems," *Journal of Magnetism and Magnetic Materials*, vol. 293, 2005, pp. 655–662.

[22] B.H. McNaughton, R.R. Agayan, J.X. Wang, and R. Kopelman, "Physiochemical microparticle sensors based on nonlinear magnetic oscillations," *Sensors & Actuators: B. Chemical*, vol. 121, 2007, pp. 330–340.

[23] K. Erglis, Q. Wen, V. Ose, A. Zeltins, A. Sharipo, P.A. Janmey, and A. Cebers, "Dynamics of Magnetotactic Bacteria in a Rotating Magnetic Field," *Biophysical Journal*, vol. 93, Aug. 2007, pp. 1402-1412.

[24] I. Sinn, P. Kinnunen, T. Albertson, B.H. McNaughton, D.W. Newton, M.A. Burns, and R. Kopelman, "Asynchronous Magnetic Bead Rotation (AMBR) biosensor in microfluidic droplets for rapid bacterial growth and susceptibility measurements," *Lab on a Chip*, 2011, p. doi:10.1039/C0LC00734J.

[25] R. Moskowitz and R.E. Rosensweig, "Nonmechanical torque-driven flow of a ferromagnetic fluid by an electromagnetic field," *Applied Physics Letters*, vol. 11, 1967, pp. 301-303.

[26] C. Caroli and P. Pincus, "Response of an isolated magnetic grain suspended in a liquid to a rotating field," *Physik der Kondensierten Materie*, vol. 9, 1969, pp. 311-319.

[27] J. Popplewell, R.E. Rosensweig, and R. Johnston, "Magnetic field induced rotations in ferrofluids," *Magnetics, IEEE Transactions on*, vol. 26, 1990, pp. 1852-1854.

[28] P. Tierno, J. Claret, F. Sagués, and A. Cemacrbers, "Overdamped dynamics of paramagnetic ellipsoids in a precessing magnetic field," *Physical Review E*, vol. 79, Feb. 2009, p. 021501.

[29] W.A. Shelton, K.D. Bonin, and T.G. Walker, "Nonlinear motion of optically torqued nanorods," *Physical Review E*, vol. 71, 2005, p. 36204.

[30] P. Valberg and J. Butler, "Magnetic particle motions within living cells. Physical theory and techniques," *Biophysical Journal*, vol. 52, Oct. 1987, pp. 537-550.

[31] R.E. Rosensweig, *Ferrohydrodynamics*, Cambridge: Cambridge University Press, 1985.

[32] G. Helgesen, P. Pieranski, and A.T. Skjeltorp, "Nonlinear phenomena in systems of magnetic holes," *Physical Review Letters*, vol. 64, Mar. 1990, p. 1425.

[33] J.C. Bacri, A. Cēbers, and R. Perzynski, "Behavior of a magnetic fluid microdrop in

a rotating magnetic field," *Physical Review Letters*, vol. 72, Apr. 1994, p. 2705.

[34] S. Lācis, J.C. Bacri, A. Cēbers, and R. Perzynski, "Frequency locking and devil's staircase for a two-dimensional ferrofluid droplet in an elliptically polarized rotating magnetic field," *Physical Review E*, vol. 55, Mar. 1997, p. 2640.

[35] G. Korneva, H. Ye, Y. Gogotsi, D. Halverson, G. Friedman, J.C. Bradley, and K.G. Kornev, "Carbon nanotubes loaded with magnetic particles," *Nano Letters*, vol. 5, 2005, pp. 879-884.

[36] G. Romano, L. Sacconi, M. Capitanio, and F.S. Pavone, "Force and torque measurements using magnetic micro beads for single molecule biophysics," *Optics Communications*, vol. 215, 2003, pp. 323-331.

[37] X.J.A. Janssen, A.J. Schellekens, K. van Ommering, L.J. van Ijzendoorn, and M.W.J. Prins, "Controlled torque on superparamagnetic beads for functional biosensors," *Biosensors and Bioelectronics*, vol. 24, 2009, pp. 1937–1941.

[38] K.M. Krishnan, "Biomedical Nanomagnetics: A Spin Through Possibilities in Imaging, Diagnostics, and Therapy," *IEEE transactions on magnetics*, vol. 46, Jul. 2010, pp. 2523-2558.

[39] B.F. Brehm-Stecher and E.A. Johnson, "Single-cell microbiology: tools, technologies, and applications," *Microbiology and Molecular Biology Reviews*, vol. 68, 2004, p. 538.

[40] A. Elfwing, Y. LeMarc, J. Baranyi, and A. Ballagi, "Observing growth and division of large numbers of individual bacteria by image analysis," *Applied and Environmental Microbiology*, vol. 70, 2004, p. 675.

[41] I. Inoue, Y. Wakamoto, H. Moriguchi, K. Okano, and K. Yasuda, "On-chip culture system for observation of isolated individual cells," *Lab on a Chip*, vol. 1, 2001, pp. 50–55.

[42] A. Touhami, M.H. Jericho, and T.J. Beveridge, "Atomic force microscopy of cell growth and division in Staphylococcus aureus," *Journal of bacteriology*, vol. 186, 2004, p. 3286.

[43] A.K. Bryan, A. Goranov, A. Amon, and S.R. Manalis, "Measurement of mass, density, and volume during the cell cycle of yeast," *Proceedings of the National Academy of Sciences*, vol. 107, 2010, p. 999.

[44] C.J. Behrend, J.N. Anker, and R. Kopelman, "Brownian modulated optical nanoprobes," *Applied Physics Letters*, vol. 84, 2004, p. 154.

[45] J.N. Anker and R. Kopelman, "Magnetically modulated optical nanoprobes," *Applied Physics Letters*, vol. 82, 2003, p. 1102.

[46] A. Vuppu, A. Garcia, and M. Hayes, "Video Microscopy of Dynamically Aggregated Paramagnetic Particle Chains in an Applied Rotating Magnetic Field," *Langmuir*, vol. 19, Oct. 2003, pp. 8646-8653.

[47] A. Rida and M.A.M. Gijs, "Manipulation of Self-Assembled Structures of Magnetic Beads for Microfluidic Mixing and Assaying," *Analytical Chemistry*, vol. 76, Nov. 2004, pp. 6239-6246.

[48] S. Miltenyi, W. Müller, W. Weichel, and A. Radbruch, "High gradient magnetic cell separation with MACS," *Cytometry*, vol. 11, 1990, pp. 231-238.

[49] O. Olsvik, T. Popovic, E. Skjerve, K.S. Cudjoe, E. Hornes, J. Ugelstad, and M. Uhlen, "Magnetic separation techniques in diagnostic microbiology.," *Clin. Microbiol. Rev.*, vol. 7, Jan. 1994, pp. 43-54.

[50] P.A. Chapman and C.A. Siddons, "A comparison of immunomagnetic separation and direct culture for the isolation of verocytotoxin-producing Escherichia coli O157 from cases of bloody diarrhoea, non-bloody diarrhoea and asymptomatic contacts," *J Med Microbiol*, vol. 44, Apr. 1996, pp. 267-271.

[51] D.R. Baselt, G.U. Lee, M. Natesan, S.W. Metzger, P.E. Sheehan, and R.J. Colton, "A biosensor based on magnetoresistance technology," *Biosensors and Bioelectronics*, vol. 13, 1998, pp. 731–739.

[52] Y.R. Chemla, H.L. Grossman, Y. Poon, R. McDermott, R. Stevens, M.D. Alper, and J. Clarke, "Ultrasensitive magnetic biosensor for homogeneous immunoassay," *Proceedings of the National Academy of Sciences of the United States of America*, vol. 97, Dec. 2000, pp. 14268 -14272.

[53] J. Connolly and T.G. St Pierre, "Proposed biosensors based on time-dependent properties of magnetic fluids," *Journal of Magnetism and Magnetic Materials*, vol. 225, 2001, pp. 156-160.

[54] Q.A. Pankhurst, J. Connolly, S.K. Jones, and J. Dobson, "Applications of magnetic nanoparticles in biomedicine," *Journal of Physics D: Applied Physics*, vol. 36, 2003, pp. R167-R181.

[55] B. Ilic, D. Czaplewski, M. Zalalutdinov, H.G. Craighead, P. Neuzil, C. Campagnolo, and C. Batt, "Single cell detection with micromechanical oscillators," *Journal of Vacuum Science & Technology B: Microelectronics and Nanometer Structures*, vol. 19, 2001, p. 2825.

[56] M. Godin, F.F. Delgado, S. Son, W.H. Grover, A.K. Bryan, A. Tzur, P. Jorgensen, K. Payer, A.D. Grossman, M.W. Kirschner, and S.R. Manalis, "Using buoyant mass to measure the growth of single cells," *Nature Methods*, vol. 7, May. 2010, pp. 387-390.

[57] S.L. Biswal and A.P. Gast, "Micromixing with linked chains of paramagnetic particles.," *Analytical chemistry*, vol. 76, 2004, p. 6448.

[58] T. Roy, A. Sinha, S. Chakraborty, R. Ganguly, and I.K. Puri, "Magnetic microsphere-based mixers for microdroplets," *Physics of Fluids*, vol. 21, 2009, p. 027101.

[59] G. Helgesen, P. Pieranski, and A.T. Skjeltorp, "Dynamic behavior of simple magnetic hole systems," *Physical Review A*, vol. 42, 1990, pp. 7271–7280.

[60] A. Ranzoni, X.J.A. Janssen, M. Ovsyanko, L.J.V. IJzendoorn, and M.W.J. Prins, "Magnetically controlled rotation and torque of uniaxial microactuators for lab-on-a-chip applications," *Lab on a Chip*, vol. 10, 2010, pp. 179-188.

[61] B.H. McNaughton, V.A. Stoica, J.N. Anker, K.M. Tyner, R. Clarke, and R. Kopelman, "Fabrication of Nanoparticles and Microspheres with Uniform Magnetic Half-Shells," *MRS Proceedings*, vol. 988, 2006, p. 899.

[62] A. Cēbers and M. Ozols, "Dynamics of an active magnetic particle in a rotating magnetic field," *Physical Review E*, vol. 73, 2006, p. 21505.

[63] B.B. Yellen and L.N. Virgin, "Nonlinear dynamics of superparamagnetic beads in a traveling magnetic-field wave," *Physical Review E*, vol. 80, Jul. 2009, p. 011402.

[64] P. Tierno, T.H. Johansen, and T.M. Fischer, "Magnetically Driven Colloidal Microstirrer," *Journal of Physical Chemistry B*, vol. 111, 2007, p. 3077.

[65] R. Dreyfus, J. Baudry, M.L. Roper, M. Fermigier, H.A. Stone, and J. Bibette, "Microscopic artificial swimmers," *Nature*, vol. 437, 2005, pp. 862–865.

[66] A.T. King, K.C. Lowe, and B.J. Mulligan, "Microbial cell responses to a non-ionic surfactant," *Biotechnology Letters*, vol. 10, 1988, pp. 177–180.

[67] W.S. Rasband, *ImageJ 1.42q*, National Institutes of Health, Bethesda, Maryland, USA, 2010.

[68] B.H. McNaughton, K.A. Kehbein, J.N. Anker, and R. Kopelman, "Sudden breakdown in linear response of a rotationally driven magnetic microparticle and application to physical and chemical microsensing," *Journal of Physical Chemistry B*, vol. 110, 2006, p. 18958.

[69] S.H. Strogatz, *Nonlinear dynamics and chaos: with applications to physics, biology, chemistry, and engineering*, Da Capo Press, 2000.

[70] H.G. Craighead, "Nanoelectromechanical systems," *Science*, vol. 290, 2000, p. 1532.

[71] K.L. Ekinci and M.L. Roukes, "Nanoelectromechanical systems," *Review of Scientific Instruments*, vol. 76, 2005, p. 061101.

[72] B. Ilic, Y. Yang, and H.G. Craighead, "Virus detection using nanoelectromechanical devices," *Applied Physics Letters*, vol. 85, 2004, p. 2604.

[73] T.P. Burg, M. Godin, S.M. Knudsen, W. Shen, G. Carlson, J.S. Foster, K. Babcock, and S.R. Manalis, "Weighing of biomolecules, single cells and single nanoparticles in fluid," *Nature*, vol. 446, 2007, pp. 1066–1069.

[74] A.M. Fennimore, T.D. Yuzvinsky, W. Han, M.S. Fuhrer, J. Cumings, and A. Zettl, "Rotational actuators based on carbon nanotubes," *Nature*, vol. 424, Jul. 2003, pp. 408-410.

[75] R.B. Bhiladvala and Z.J. Wang, "Effect of fluids on the Q factor and resonance frequency of oscillating micrometer and nanometer scale beams," *Physical Review E*, vol. 69, Mar. 2004, p. 036307.

[76] M.R. Paul and M.C. Cross, "Stochastic Dynamics of Nanoscale Mechanical Oscillators Immersed in a Viscous Fluid," *Physical Review Letters*, vol. 92, Jun. 2004, p. 235501.

[77] J.F. Vignola, J.A. Judge, J. Jarzynski, M. Zalalutdinov, B.H. Houston, and J.W. Baldwin, "Effect of viscous loss on mechanical resonators designed for mass detection," *Applied Physics Letters*, vol. 88, 2006, p. 041921.

[78] B.L. Weeks, J. Camarero, A. Noy, A.E. Miller, J.J. De Yoreo, and L. Stanker, "A microcantilever-based pathogen detector," *Scanning*, vol. 25, 2003, pp. 297-299.

[79] K.Y. Gfeller, N. Nugaeva, and M. Hegner, "Rapid Biosensor for Detection of Antibiotic-Selective Growth of Escherichia coli," *Appl. Environ. Microbiol.*, vol. 71, May. 2005, pp. 2626-2631.

[80] "CDC - Get Smart: Antibiotic Resistance Questions and Answers," *Get Smart: Know When Antibiotics Work* Available: http://www.cdc.gov/getsmart/antibiotic-use/anitbiotic-resistance-faqs.html.

[81] J.J. Kerremans, P. Verboom, T. Stijnen, L. Hakkaart-van Roijen, W. Goessens, H.A. Verbrugh, and M.C. Vos, "Rapid identification and antimicrobial susceptibility test-

ing reduce antibiotic use and accelerate pathogen-directed antibiotic use," *Journal of Antimicrobial Chemotherapy*, vol. 61, Feb. 2008, pp. 428 -435.

[82] S.E. Cosgrove, "The Relationship between Antimicrobial Resistance and Patient Outcomes: Mortality, Length of Hospital Stay, and Health Care Costs," *Clinical Infectious Diseases*, vol. 42, 2006, pp. S82-S89.

[83] C.H. Chen, Y. Lu, M.L.Y. Sin, K.E. Mach, D.D. Zhang, V. Gau, J.C. Liao, and P.K. Wong, "Antimicrobial Susceptibility Testing Using High Surface-to-Volume Ratio Microchannels," *Analytical Chemistry*, vol. 82, Feb. 2010, pp. 1012-1019.

[84] G.V. Doern, R. Vautour, M. Gaudet, and B. Levy, "Clinical impact of rapid in vitro susceptibility testing and bacterial identification.," *Journal of Clinical Microbiology*, vol. 32, Jul. 1994, pp. 1757-1762.

[85] Y. Nagaoka, H. Morimoto, and T. Maekawa, "Dynamics of disklike clusters formed in a magnetorheological fluid under a rotational magnetic field," *Physical Review E*, vol. 71, 2005.

[86] S. Melle, O.G. Calderón, M.A. Rubio, and G.G. Fuller, "Microstructure evolution in magnetorheological suspensions governed by Mason number," *Physical Review E*, vol. 68, Oct. 2003, p. 041503.

[87] Q. Chen, S.C. Bae, and S. Granick, "Directed self-assembly of a colloidal kagome lattice," *Nature*, vol. 469, Jan. 2011, pp. 381-384.

[88] E. Climent, K. Yeo, M.R. Maxey, and G.E. Karniadakis, "Dynamic Self-Assembly of Spinning Particles," *Journal of Fluids Engineering*, vol. 129, Apr. 2007, pp. 379-387.

[89] J.C. Bacri, A. Cēbers, S. Lācis, and R. Perzynski, "Dynamics of a magnetic fluid droplet in a rotating field," *Journal of Magnetism and Magnetic Materials*, vol. 149, Aug. 1995, pp. 143-147.

[90] B. Kavčič, D. Babič, N. Osterman, B. Podobnik, and I. Poberaj, "Magnetically actuated microrotors with individual pumping speed and direction control," *Applied Physics Letters*, vol. 95, 2009, p. 023504.

[91] S. Bleil, D.W.M. Marr, and C. Bechinger, "Field-mediated self-assembly and actuation of highly parallel microfluidic devices," *Applied Physics Letters*, vol. 88, 2006, p. 263515.

[92] B.A. Grzybowski, H.A. Stone, and G.M. Whitesides, "Dynamic self-assembly of magnetized, millimetre-sized objects rotating at a liquid-air interface," *Nature*, vol. 405, Jun. 2000, pp. 1033-1036.

[93] Center for Devices and Radiological Health, "Guidance Documents (Medical Devices and Radiation-Emitting Products) - Class II Special Controls Guidance Document: Antimicrobial Susceptibility Test (AST) Systems" Available: http://www.fda.gov/MedicalDevices/DeviceRegulationandGuidance/GuidanceDocuments/ucm080564.htm.

[94] Bangs Laboratories, Inc., "TechNote 204: Adsorption to Microspheres" Available: http://www.bangslabs.com/files/bangs/docs/pdf/204.pdf.

[95] I. Sinn, P. Kinnunen, S.N. Pei, R. Clarke, B.H. McNaughton, and R. Kopelman, "Magnetically uniform and tunable Janus particles," *Applied Physics Letters*, vol. 98, 2011, p. 024101.

[96] J.L. Neuringer and R.E. Rosensweig, "Ferrohydrodynamics," *Physics of Fluids*, vol. 7, 1964, p. 1927.